3-D volumetric Lensfree imaging using Digital Holographic Microscopy

Ashish Chakole

A Dissertation Submitted to

Indian Institute of Technology Hyderabad

In Partial Fulfillment of the Requirements for

The Degree of Master of Technology

भारतीय प्रौद्योगिकी संस्थान हैदराबाद

Indian Institute of Technology Hyderabad

Department of Biomedical Engineering

June, 2015

Declaration

I declare that this written submission represents my ideas in my own words, and where others' ideas or words have been included, I have adequately cited and referenced the original sources. I also declare that I have adhered to all principles of academic honesty and integrity and have not misrepresented or fabricated or falsified any idea/data/fact/source in my submission. I understand that any violation of the above will be a cause for disciplinary action by the Institute and can also evoke penal action from the sources that have thus not been properly cited, or from whom proper permission has not been taken when needed.

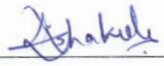

(Signature)

Ashish Chakole

(– Student Name –)

BM13M1001

(Roll No)

Approval Sheet

This thesis entitled 3-D volumetric Lensfree imaging using Digital Holographic Microscopy by Ashish Chakole is approved for the degree of Master of Technology from IIT Hyderabad.

Harikrishnan

Dr. Harikrishnan. N. Unni
Internal Examiner

Dr. Renu John
Associate Professor and Head
Department of Biomedical Engineering
Indian Institute of Technology, Hyderabad

Vandana Sharma

(Dr. V. Sharma,
Physics Dept.)

Acknowledgements

I would like to express my special appreciation and thanks to my advisor Professor Dr. RENU JOHN, Associate professor, Department of Biomedical Engineering, IIT Hyderabad, for encouraging me at every moment which helped me achieving my goals. I am grateful to my mentor Mr. Vimal Prabhu, PhD scholar, for sharing expertise, and sincere and valuable guidance throughout my course. I would also like to thank Mr. Hanu Phani Ram, PhD scholar, for his kind support. I'm grateful to my classmates and friends for backing me in hard time.

I take this opportunity to express gratitude to my parents for the unceasing encouragement, support and attention.

Dedicated to

My Parents and Loved ones.

Abstract

Despite of advancement in microscopic techniques most of the improved microscopy modalities are complex, bulky and require costly setup. Many of the modalities are not capable of live imaging. Today imaging devices are needed to be compact, cost-effective, portable, light-weight and significantly accurate and easy to handle. Digital holography has overcome few barriers but still demands costly setup. Here we demonstrate the lensfree imaging which is based on "Digital In-line holography" principle and does not require bulky and costly setup. The technique uses Light emitting diode (LED) as a source of light and CCD camera to capture the hologram of the object which allow to reconstruct the image using numerical algorithm on computing machines. This technique has many applications including one in telemedicine and can address the issues related to the rural health.

Nomenclature

ρ	Distance between a point in hologram plane to a point in reconstruction plane
D	Reconstruction distance from hologram plane to reconstruction plane
$\mathfrak{F}_r$	Fresnel transformation operator
$\Delta x, \Delta y$	Pixel sizes in x and y direction in hologram plane
k_x, k_y	Wave vector components in x and y-directions respectively.
D	Radius of curvature which adjusts the curvature of the wave field
$\odot$	Convolution operator
$\Phi(\xi, \eta)$	Digital phase mask
DHM	Digital Holographic Microscopy
ϕ	Phase angle
E_0	Light wave of object wave
E_R	Light wave of reference wave
E_R^*	Light wave of conjugate reference wave
H	Hologram
$\Gamma(\xi, \eta)$	Reconstruction field
(ξ, η)	Co-ordinates in object plane
(x, y)	Co-ordinates in hologram plane
(ξ', η')	Co-ordinates in reconstruction plane
λ	Wavelength of light
I(x,y)	intensity

List of figures

Contents

Chapter 1

Introduction

For years, optical microscopy has been the backbone of various fields including engineering, medicine, physical sciences, and biology. Despite its long history, until recently, there has not been a noteworthy change in the construction and working principles of optical microscopes. Over the last decade, driven partially by the research to better understand the kingdom of the nano-world, super-resolution techniques started a revival for optical microscopy by addressing some of the most fundamental limitations of optical imaging such as the diffraction limit. Apart from these super-resolution techniques, several other innovative imaging architectures were also implemented to improve the state of the art in optical microscopy towards better speed, contrast, throughput, signal to noise ratio (SNR), specificity, etc. [1]–[4]

This recent progress in microscopy used various innovative technologies to overcome the fundamental barriers in imaging and has created significant excitement in a diverse set of fields by allowing new discoveries to be made. However, together with this progress, the overall complexity and the cost of the optical imaging platform relatively increased which limits the wide spread use of some of these cutting-edge optical imaging modalities beyond well-equipped laboratories. In the meantime, we have been also experiencing a speedy advancement in digital technologies, with much cheaper 2D solid state detector arrays having significantly larger areas with smaller pixels, better dynamic ranges, frame rates and signal to noise ratios, as well as much faster, cheaper and more powerful digital processors and memories. This current digital revolution, when combined with advanced imaging theories and numerical algorithms, also creates an opportunity for optical imaging and microscopy to face another dimension in this revival towards simplification of the optical imaging apparatus, making it ominously more compact, cost-effective and easy to use, possibly without a trade-off in its performance. As we illustrate in this document, lensfree incoherent holographic on-

chip imaging can be considered to be at the core of this new opportunity and when combined with the advanced state of the art and cost-effective nature of digital electronics, it can provide a transformative solution to some of the unmet needs of cell biology and medical diagnostics especially for resource-limited environments. Over the last decade various lensfree on-chip imaging architectures were also revealed.[5]–[9]Among these approaches, lensfree digital holography deserves a special attention since with new computational algorithms and mathematical models, it has the potential to make the most out of this digital rev lensfree digital in-line holography has already been successfully demonstrated for high-resolution microscopy of cells and other microorganisms.[5] Conventional coherent lensfree in-line holography methods demand near-perfect spatial coherence for illumination, and thus require focusing of a laser light on a small aperture that is on the order of a wavelength for spatial filtering. The use of a small aperture size (e.g., 1–2mm) requires a mechanically stable and a cautiously aligned system together with a focusing lens to efficiently couple the laser radiation to the aperture for better light throughput. In addition, keeping such a small aperture clean and operational over a long period of time can be another challenge particularly for field use. The cells of interest are typically positioned far away (e.g., >1 cm) from the sensor surface such that the holographic signature of each cell is spread almost over the complete sensor area, where all the cells 'signatures significantly overlap. Such a method unfortunately limits the imaging field-of-view (FOV) at the cell plane. All these requirements not only relatively increase the cost and the size of the optical instrument, but also make lensfree coherent in-line holography somewhat inconvenient for use in resource inadequate settings. Incoherent or partially coherent sources in holography have also been used in different lens-based optical architectures. These holographic imaging techniques are not on-chip as they utilize various bulky optical components and therefore they can be considered under the same category as the advanced imaging modalities discussed in the introduction making them much less suitable for field use. Simpler methods using partially coherent or incoherent lensfree in-line holography have also been recently demonstrated for imaging of latex particles. However, these methods also suffer from a small field-of-view as they place the objects-of-interest far away from the sensor surface, e.g., with a fringe magnification of >10, reducing the available field-of-view of the digital sensor by more than two orders of magnitude. Further, these studies used coupling optics for the illumination such as a microscope objective-lens and had relatively coarse imaging performance.

1.1 Optical microscopy

The history of microscopy started with the use of compound microscope by Robert Hooke to observe pores in cork which he called them as cells. Antoine van Leeuwenhoek is the first person to see the single celled organisms in pond water using the microscope. He used only single converging lens for magnification. In 1658, Jan Swammerdam observed erythrocytes with single lens microscopy. His main work was to observe the bodies of the insects at different stages of development. Marcello Malpighi observed brain, blood vessels, tongue, retina and development of chicken embryo. Johannes Evangelista Purkinje used the compound microscopy to discover purkinje neurons in cortex of cerebellum, sweat glands in skin, purkinje fibers in heart. In 1873, abbe formulated limit for optical resolution related to the wavelength of the incident light and numerical aperture. Thus, many researchers started exploring the microscopes. Bright field microscopy is the simplest and the oldest microscopic technique where the dark contrast to the bright background will be obtained by absorption of the light by the sample. It can be used to observe fixed as well as live cells. As cells are transparent to the light staining is required to improve the contrast. The staining may result in artifacts. The resolution of the bright field microscope is limited to 0.2 μm. So, bright field microscopy is best suitable for the amplitude objects. Phase objects cannot be seen properly in bright field microscopy. In Dark field microscope, bright sample is formed against the dark background. Here, a filter is used to remove the non-diffracted light, the image contains only the diffracted light. It is used to image bacteria, flagella, microtubules, actin filaments, unstained specimens. Thus, dark field microscope is good for light scattering specimens. Thus, bright field and dark field microscopic techniques are not good for phase objects like cells; phase information is utilized by Zernike for imaging using phase contrast microscopy. Thus phase changes are detected by Zernike with the invention of phase contrast microscopy in early 1930's. In phase contrast microscopy the phase information is converted to amplitude information. When light is incident upon the phase objects, zeroth order light passes through the specimen without deviation. Other wave is the diffracted wave, usually diffracted wave and non-diffracted wave has phase difference of $\lambda/4$. The diffracted light is delayed to non-diffracted light by $\lambda/4$. If a phase ring of phase delay $\lambda/4$ is introduced to the diffracted light then total phase delay between diffracted and non-diffracted light would be $\lambda/2$. Then they both interfere it would create a destructive interference which would make the sample dark with bright background. This is known as positive phase contrast. This is the principle for Zernike phase contrast microscopy. This method is not suitable for the thick specimens as thick materials appear distorted under phase contrast microscope.

Chapter 2

Digital holography

2.1 Introduction

In 1948, Dennis Gabor, a British scientist introduced "A new microscopic principle", as a method for recording and reconstructing amplitude and phase of wave while working to improve resolution of electron microscope[10]–[12]. He termed it as 'holography' from the Greek words 'halos' meaning whole or entire and 'graphein' meaning to write. A hologram is the photographically recorded interference pattern between a wave field scattered from the object and a reference wave which is a coherent background. An entire 3-dimensional wave field is recorded on a flat surface. The data is coded in the form of interference patterns which contain high spatial frequencies and cannot be seen by human eyes. Reconstruction of the image is carried out by illuminating the hologram by reference wave again. Reconstructed image can be recognized by effects of perspective and depth of focus[13].

Further development of holography was obstructed for few years after the invention due to unavailability of coherent sources. In 1960, N. Bassov, A. Prokhorov, and Charles Towns invented laser whose pure, intense light was ideal in order to make holograms. In the same year, Pulsed-Ruby laser was developed by Dr. T. H. Maimam to emit powerful burst of light for a few nanoseconds which made it possible to record high-speed events. In 1967, first hologram of the person was made which paved the way for a specialized application of holography. Dr. Stephen A. Benton, in 1968 invented white-light transmission holography by which hologram can be viewed in ordinary white light creating rainbow image from the seven colors which take up white light. Lloyd Cross in 1972 combined white light transmission holography with conventional cinematography and produced 3-D images.

Gabor illuminated hologram by a parallel beam through the transparent objects where object beam and reference beams were parallel, i.e. in-line holography, where the real image is superimposed by un-diffracted part of reconstruction wave resulting in 'tween image'. Leith

and Upatnieks introduced an off axis reference wave to avoid twin image problem[14], [15]. Goodman and Lawrence[16] and Yaroslavskii, Merzlyakov and Kronrod[17] introduced numerical hologram reconstruction.

Schnars and Juptner developed direct recording of Fresnel's holograms with charged coupled Devices which brought revolution in the field of holography[18], [19]. Later on this method was termed as "Digital Holography".

2.2 Holography

2.2.1 Recording and Reconstruction

Holograms are recorded using optical set-up which is consist of a light source, mirrors, lenses

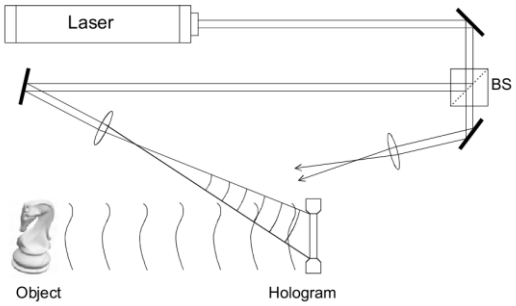

Figure 2-1 : Hologram Recording [13]

and beam splitters. Generally photographic plate is used to record the image in conventional holography. A typical optical set-up is shown in Figure 2-1[13]. Coherent light is split into two beams using beam splitter. One of the beams illuminates the object and reflects back to the recording medium after getting scattered. Another beam illuminates light sensitive medium directly. Both beams interfere at a plane and the interference pattern is recorded on photographic plate.

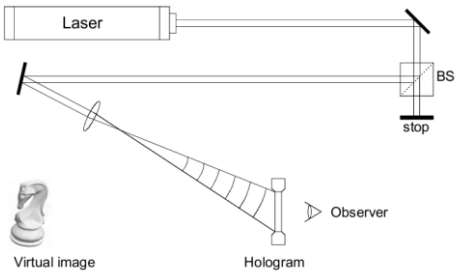

Figure 2-2 : Hologram Reconstruction [13]

Object is reconstructed using reference wave by illuminating the hologram, Figure 2-2. Reconstructed image contain all effects of depth of focus. Holographic method can be described mathematically as shown

The complex amplitude of the object wave is given by:

$$E_0(x,y) = a_0(x,y)\, exp\big(i\varphi_0(x,y)\big) \tag{2.1}$$

Where a_0 is amplitude and φ_0 is phase

Complex amplitude of reference wave with real amplitude a_R and phase φ_0 is given by:

$$E_R(x,y) = a_R(x,y)\, exp\big(i\varphi_0(x,y)\big) \tag{2.2}$$

Object and reference waves interfere at the recording medium, and the intensity is calculated by,

$$I(x,y) \;= |E_0(x,y) + E_R(x,y)|^2 \tag{2.3}$$

$$= (E_0(x,y) + E_R(x,y))\,(E_0(x,y) + E_R(x,y))^* \tag{2.4}$$

$$= E_R(x,y){E_R}^*(x,y) + E_0(x,y){E_0}^*(x,y) + E_0(x,y){E_R}^*(x,y) + E_R(x,y){E_0}^*(x,y) \tag{2.5}$$

The amplitude transmission $h(x,y)$ is proportional to $I(x,y)$:

$$h(x,y) = h_0 + \beta\tau I(x,y) \tag{2.6}$$

$h(x,y)$ is hologram function. β is an amplitude of transmittance versus exposure characteristics material and it is negative for photographic emulsions. h_0 is the amplitude transmission of the unexposed plate which can be neglected in digital holography and τ is the exposure time

In order to reconstruct hologram, amplitude transmission is multiplied with complex amplitude of the reference wave

$$E_R(x,y)h(x,y) =$$

$$[h_0 + \beta\tau(a_r^2 + a_0^2)]E_R(x,y) + \beta\tau a_R^2 E_0(x,y) + \beta\tau E_R^2(x,y)E_0^*(x,y) \tag{2.7}$$

First term in the right side equation is reference wave multiplied by the factor which represents zero diffraction order. Second term refers to the virtual image which is reconstructed object wave. The third term is responsible for the distorted real image of the object. An undistorted image can be generated by conjugate reference beam E_R^* for reconstruction.

$$E_R^*(x,y)h(x,y) =$$

$$[h_0 + \beta\tau(a_r^2 + a_0^2)]E_R^*(x,y) + \beta\tau a_R^2 E_0^*(x,y) + \beta\tau E_R^{*2}(x,y)E_0(x,y) \tag{2.8}$$

2.3 Image Equations

If hologram is reconstructed using same parameters which are used in recording then the position of the virtual image will appear at the original position of the object. If one changes the wavelength or coordinates of the reference wave the reconstructed image moves. The

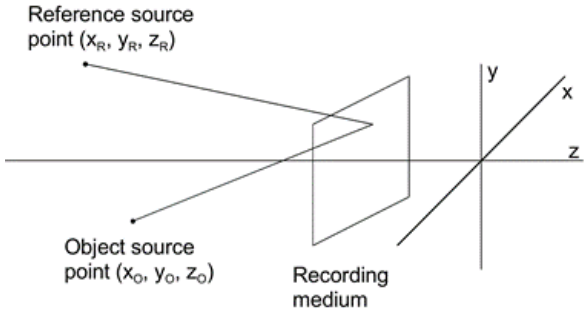

Figure 2-3 : Coordinate system for hologram recording [13]

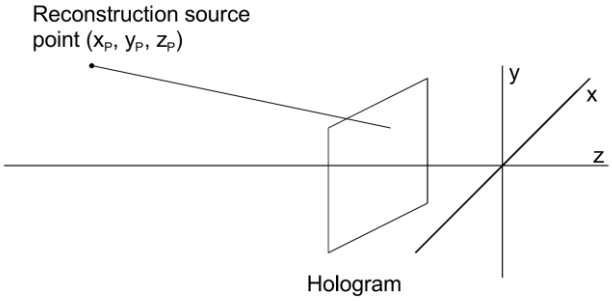

Figure 2-4 : Coordinate system for hologram reconstruction [13]

shape of the reconstructed image gets distorted if the coordinate shift is different for all points. The image magnification can be influenced by reconstruction parameters

The coordinate system is shown in Figure 2-8(x_0, y_0, z_0) are the coordinates of the object point O, (x_R, y_R, z_R) are the coordinates of the source point of the reference wave used for hologram recording and $(x_P, y_P, z_{P)}$ are the coordinates of the source point of reference wave. $\mu = \lambda_2/\lambda_1$ denotes the ratio between the recording wavelength λ_1 and the reconstruction wavelength λ_2. The coordinate corresponds to object point O, are:

$$x_1 = \frac{x_P z_0 z_R + \mu x_0 z_P z_R - \mu x_R z_P z_0}{z_0 z_R + \mu z_P z_R - \mu z_P z_0} \tag{2.9}$$

$$y_1 = \frac{y_P z_0 z_R + \mu y_0 z_P z_R - \mu y_R z_P z_0}{z_0 z_R + \mu z_P z_R - \mu z_P z_0} \tag{2.10}$$

$$z_2 = \frac{z_P z_0 z_R}{z_0 z_R - \mu z_P z_R + \mu z_P z_0} \tag{2.11}$$

Coordinates in the real image those correspond to object point O, are:

$$x_2 = \frac{x_P z_0 z_R - \mu x_0 z_P z_R + \mu x_R z_P z_0}{z_0 z_R - \mu z_P z_R + \mu z_P z_0} \tag{2.12}$$

$$y_2 = \frac{y_P z_0 z_R - \mu y_0 z_P z_R + \mu y_R z_P z_0}{z_0 z_R - \mu z_P z_R + \mu z_P z_0} \tag{2.13}$$

$$z_2 = \frac{z_P z_0 z_R}{z_0 z_R - \mu z_P z_R + \mu z_P z_0} \tag{2.14}$$

Considering object made up of point objects, lateral magnification of the entire virtual image is as follows:

$$M_{lat,1} = \frac{dx_1}{dx_0} = \left[1 + z_0\left(\frac{1}{\mu z_P} - \frac{1}{z_R}\right)\right]^{-1} \tag{2.15}$$

Lateral magnification of the real image results in:

$$M_{lat,2} = \frac{dx_2}{dx_0} = \left[1 - z_0\left(\frac{1}{\mu z_P} + \frac{1}{z_R}\right)\right]^{-1} \tag{2.16}$$

The longitudinal magnification of the virtual image is given by:

$$M_{long,1} = \frac{dz_1}{dz_0} = \frac{1}{\mu} M_{lat,1}^2 \tag{2.17}$$

The longitudinal magnification of the real image is:

$$M_{long,2} = \frac{dz_2}{dz_0} = -\frac{1}{\mu} M_{lat,2}^2 \tag{2.18}$$

Real image is formed by conjugate object wave O^*, its depth is inverted. Corresponding point of real and virtual image are located at equal distance from the hologram plane, but at opposite side of it.

2.4 Digital Holography

2.4.1 General Principles

A reference wave and the wave reflected from object interfere at the surface of charged couple Device (CCD) as shown in Figure 2-5. The hologram is recorded and stored. The 3-dimensional object is located at a distance d from CCD.

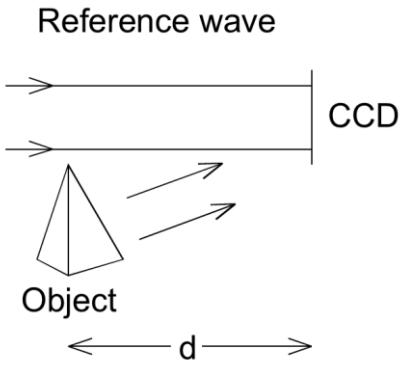

Figure 2-5 : Recording [20]

In reconstruction the virtual image appears at the position of the original object and real image at distance d in opposite direction as shown in Figure 2-6. The diffraction of a light wave

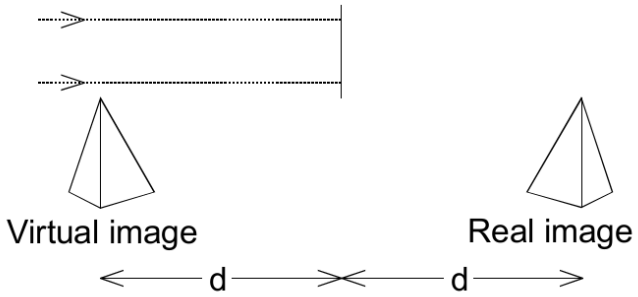

Figure 2-6 : Reconstruction with reference wave [20]

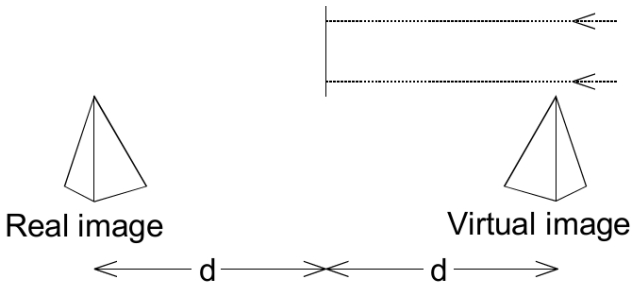

Figure 2-7 : Reconstruction with conjugate reference wave [13]

mounted perpendicular to the incoming beam which is described by the Fresnel-Kirchhoff integral as shown in eq. 2.19

$$\Gamma(\xi',\eta') = \frac{i}{\lambda}\int_{-\infty}^{\infty}\int_{-\infty}^{\infty} h(x,y)E_R(x,y)\frac{\exp\left(-i\frac{2\pi}{\lambda}\rho'\right)}{\rho'}dxdy \qquad (2.19)$$

With,

$$\rho' = \sqrt{(x-\xi')^2 + (y-\eta')^2 + d^2} \qquad (2.20)$$

$h(x, y)$ is the hologram function and ρ' is the distance between a point in the hologram plane and a point in the reference plane. Geometrically it is explained in Figure 2-7. Since θ and θ' are approximately 0, inclination factor is set to zero.

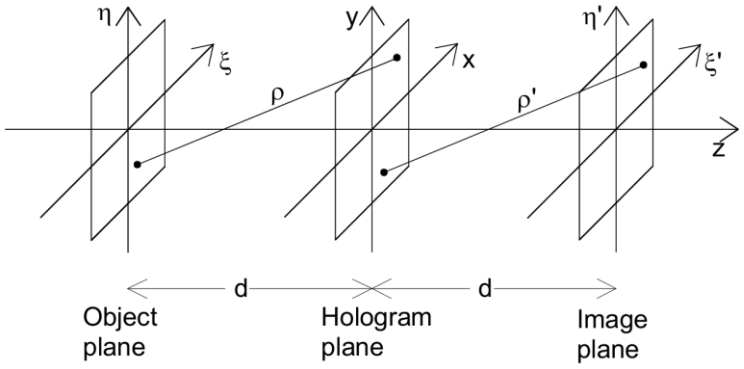

Figure 2-8 : Coordinate system for numerical hologram reconstruction [21]

For a plain reference wave,

$$E_R = a_R + io = a_R \tag{2.21}$$

The diffraction pattern is calculated behind the CCD plane at a distance d, it reconstructs the complex amplitude in plane of real image. Eq. 2.19 gives the basis of numerical hologram reconstruction. Since the reconstructed wave field is $\Gamma(\xi', \eta')$ is a complex function, both intensity as well as phase can be calculated[22].

An undistorted real image can be produced using conjugate reference beam for reconstruction. Therefore E_R^* should be inserted instead of E_R in eq. 2.19

$$\Gamma(\xi', \eta') = \frac{i}{\lambda} \int_{-\infty}^{\infty} \int_{-\infty}^{\infty} h(x, y) E_R^*(x, y) \frac{\exp\left(-i \frac{2\pi}{\lambda} \rho\right)}{\rho} dxdy \tag{2.22}$$

With,

$$\rho = \sqrt{(x - \xi)^2 + (y - \eta)^2 + d^2} \tag{2.23}$$

Reconstruction of virtual image is also possible by introducing the imaging properties of the lens into numerical reconstruction process[23]. The lens is located directly behind the hologram in simple cases, as shown in Figure 2-9

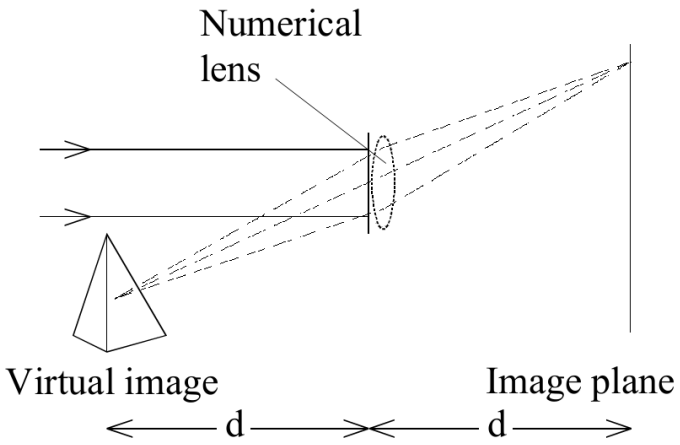

Figure 2-9 : Reconstruction of the virtual image [21]

Properties of lens with focal length as f can be considered by following eq.

$$L(x,y) = \exp\left[i\frac{\pi}{\lambda f}\,(x^2+y^2)\right] \tag{2.24}$$

$f = d/2$ is used for a magnification of 1.

2.5 Off-axis holography

The recording set-up for Off-Axis holography is shown in Figure 2-10 [15]. The offset angle

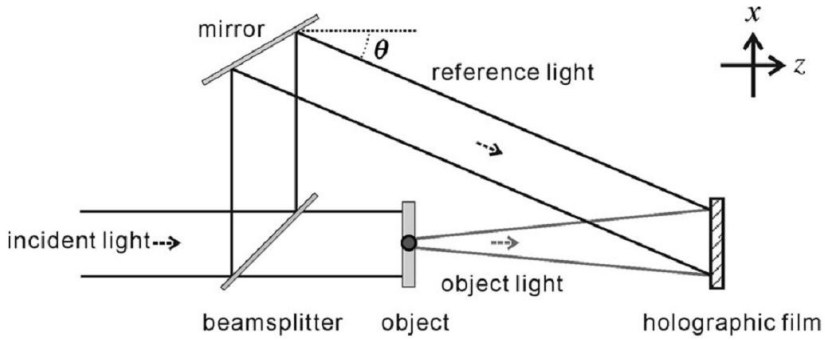

Figure 2-10: Recording setup [15]

θ is set between reference light with respect to recording film axis. Assuming propagation vector in (x-z) plane the expression for off-axis hologram is given by,

$$t(x,y) = \left|\psi_0(x,y) + \psi_r\, e^{jk_0 sin\theta x}\right|^2$$
$$= |\psi_0(x,y)|^2 + |\psi_r|^2 + \psi_0(x,y)\psi_r^*\, e^{-jk_0 sin\theta x} + \psi_0^*(x,y)\psi_r\, e^{jk_0 sin\theta x} \tag{2.25}$$

Where $\psi_0(x,y)$ and $\psi_r\, e^{jk_0 sin\theta x}$ are the complex amplitudes of object wave and reference wave respectively. $f_x = sin\theta/\lambda$ is spatial carrier frequency of hologram.

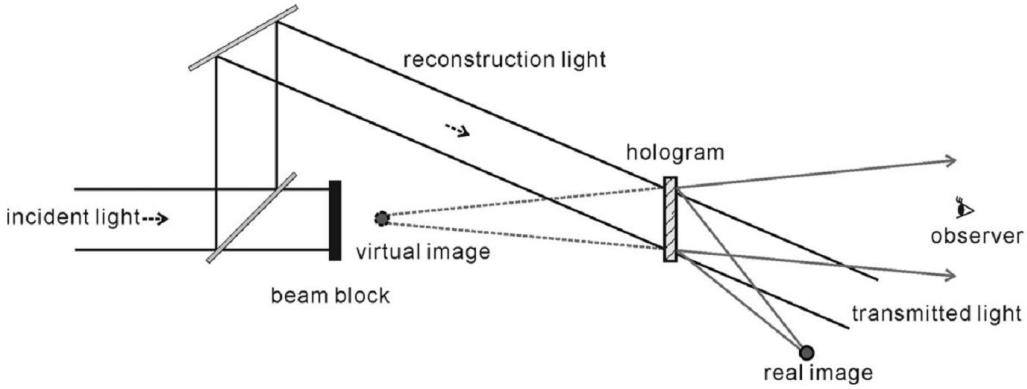

Figure 2-11 : Reconstruction setup for off-axis [15]

In reconstruction, hologram is illuminated by the reconstruction light along the direction of reference wave as shown in Figure 2-12 The complex field behind the hologram can be expressed as:

$$\Psi_r\, e^{jk_0 sin\theta x} \times t(x,y) = |\Psi_r|^2 \Psi_r\, e^{jk_0 sin\theta x} + |\Psi_0(x,y)|^2 \Psi_r\, e^{jk_0 sin\theta x} + \Psi_0(x,y)|\Psi_r|^2 + \Psi_0^*(x,y)\, \Psi_r^2 e^{j2k_0 sin\theta x} \quad (2.26)$$

The first two terms on right side represent the transmitted light i.e. zeroth-order beam. Third term gives the virtual reconstructed image and last term gives the conjugate real image.

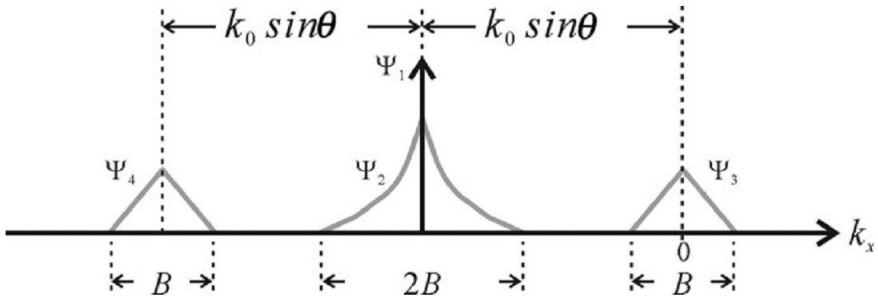

Figure 2-12 : One-dimensional plot of the spectrum of the off-axis hologram [15]

In Figure 2-12 the bandwidths of Ψ_3 and Ψ_4 are considered to be *B*, thus bandwidth of $\Psi_2$is *2B.* Therefore spectrum of the virtual image can be isolated provided off-axis angle θ is sufficiently large. To avoid overlapping of spectra Ψ_2 and Ψ_3

$$k_0 sin\theta \geq \frac{3}{2} B$$

Thus, minimum offset angle is calculated as

$$\theta_{min} = \sin^{-1}\left(\frac{3B}{2k_0}\right) \quad (2.27)$$

2.6 Numerical Reconstruction

2.6.1 Reconstruction by the Fresnel Approximation

The Fresnel approximation or Fresnel transformation is given below. It has mathematical similarity with Fourier Expression, It enables reconstruction of the wave in a plane behind the hologram here it is plane of real image.

$$\Gamma(\xi,\eta) = \frac{i}{\lambda d}\exp\left(-i\frac{2\pi}{\lambda}d\right)\exp\left[-i\frac{\pi}{\lambda d}(\xi^2+\eta^2)\right] \times \int_{-\infty}^{\infty}\int_{-\infty}^{\infty} h(x,y)E_R^*(x,y)\,exp\left[-\frac{i\pi}{\lambda d}((\xi-x)^2+(\eta-y)^2)\right]dxdy \qquad (2.28)$$

The intensity is calculated as follows:

$$I(\xi,\eta) = |\Gamma(\xi,\eta)|^2 \qquad (2.29)$$

And phase is given by,

$$\Phi(\xi,\eta) = arctan\frac{Im[\Gamma(\zeta,\eta)]}{Re[\Gamma(\zeta,\eta)]} \qquad (2.30)$$

Re denotes real part and Im denotes imaginary part.

The discrete Fresnel transform is given by:

$$\Gamma(\mathrm{m},\mathrm{n}) = \frac{\mathrm{i}}{\lambda \mathrm{d}}exp\left(-i\frac{2\pi}{\lambda}\,d\right)exp\left[-i\pi\lambda d\,\left(\frac{m^2}{N^2\Delta x^2}+\frac{n^2}{N^2\Delta y^2}\right)\right] \times \sum_{k=0}^{N-1}\sum_{l=0}^{N-1} E_R^*(k,l)h(k,l)exp\left[-i\frac{\pi}{\lambda d}\,(k^2\Delta x^2+l^2\Delta y^2)\right]exp\left[i2\pi\left(\frac{km}{N}+\frac{ln}{N}\right)\right] \qquad (2.31)$$

The matrix Γ is calculated by multiplying $E_R^*(k,l)$ with $h(k,l)$ and $exp\,[-i\pi/(\lambda d)(k^2\Delta x^2 + l^2\Delta y^2)]$ and applying an inverse discrete Fourier transform to the product. The effective calculation can be done using FFT (Fast Fourier Transform) algorithm.

The intensity is calculated as follows:

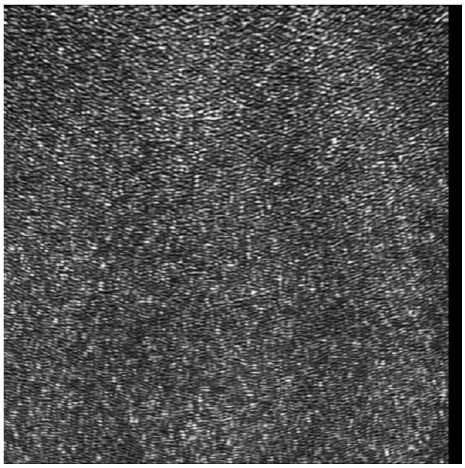

Figure 2-13 : Digital hologram[21]

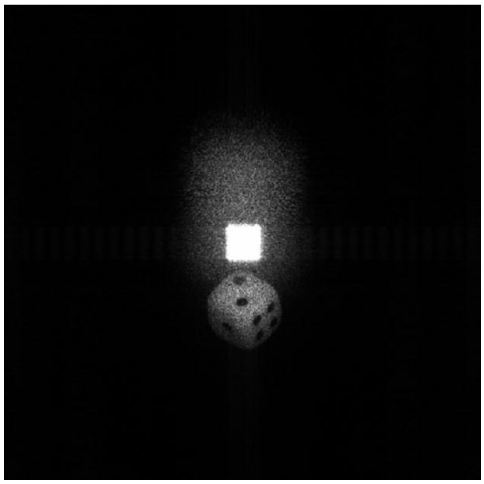

Figure 2-14 : Numerical intensity reconstruction[21]

$$\Gamma(\mathrm{m},\mathrm{n}) = \frac{\mathrm{i}}{\lambda \mathrm{d}} exp\left(-i\frac{2\pi}{\lambda}\ d\right) exp\left[+i\pi\lambda d\ \left(\frac{m^2}{N^2\Delta x^2} + \frac{n^2}{N^2\Delta y^2}\right)\right]$$

$$\times \sum_{k=0}^{N-1}\sum_{l=0}^{N-1} E_R(k,l)h(k,l)exp\left[+i\frac{\pi}{\lambda d}\ (k^2\Delta x^2 + l^2\Delta y^2)\right] exp\left[i2\pi\left(\frac{km}{N} + \frac{ln}{N}\right)\right] \qquad (2.32)$$

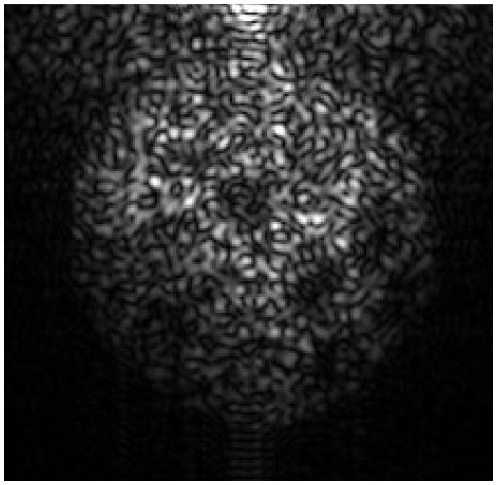

Figure 2-15 : Reconstruction with only 256 ×256 pixels[21]

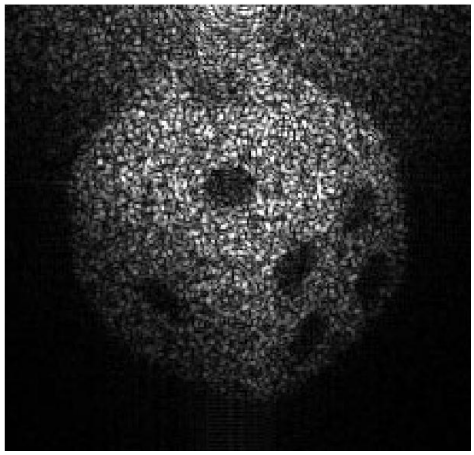

Figure 2-16 :Reconstruction with only 512×512 pixels[21]

A typical digital hologram is shown in Figure 2-13and numerical reconstruction is shown in Figure 2-14. The interesting property of hologram is that every part of hologram contains information of entire object. That is illustrated in Figure 2-15and Figure 2-16with black mask cover nearly half of the area[13]

2.6.2 Reconstruction by convolution approach

Numerical processing Fresnel-Kirchhoff equation without approximation is time consuming. For numerical process some equivalent formulation is needed. This formulation uses the convolution theorem thus it is named as "convolution approach". Demetrakopoulos and Mittra applied this kind of processing for numerical reconstruction of sub optical holograms

for the first time in 1974[24]. The reconstruction formula can be interpreted as superposition of integral:

$$\Gamma(\xi,\eta) = \int_{-\infty}^{\infty}\int_{-\infty}^{\infty} h(x,y)E_R^*(x,y)\, g(\xi,\eta,x,y)dxdy \tag{2.33}$$

Where the impulse response $g(x,y,\zeta,\eta)$ is given by

$$g(x,y,\xi,\eta) = \frac{\frac{i}{\lambda}\exp\left[-i\frac{2\pi}{\lambda}\sqrt{d^2+(x-\xi)^2+(y-\eta)^2}\right]}{\sqrt{d^2+(x-\xi)^2+(y-\eta)^2}} \tag{2.34}$$

The numerical realization of the impulse response function is

$$g(k,l) = \frac{\frac{i}{\lambda}\exp\left[-i\frac{2\pi}{\lambda}\sqrt{d^2+\left(k-\frac{N}{2}\right)^2\Delta x^2+\left(l-\frac{N}{2}\right)^2\Delta y^2}\right]}{\sqrt{d^2+\left(k-\frac{N}{2}\right)^2\Delta x^2+\left(l-\frac{N}{2}\right)^2\Delta y^2+(y-\eta)^2}} \tag{2.35}$$

Above eq. saves one Fourier transform for reconstruction. The pixel size of images reconstructed by convolution method are equal to that of hologram:

$$\Delta\xi = \Delta x; \qquad \Delta\eta = \Delta y \tag{2.36}$$

Reconstruction of holograms by the convolution approach result in images with more or less pixels per unit length than those reconstructed by the Fresnel approximation. The convolution approach is advantageously applied to reconstruct in-line holograms from particle distributions within transparent media.

2.6.3 Digital Fourier Holography

This recording geometry has been named as 'lensless Fourier holography'. It is realized in digital holography. The point of source is located in the plane of object. The reference wave at CCD plane is therefore described by:

$$\begin{aligned} E_R &= \frac{\exp\left(-i\frac{2\pi}{\lambda}\sqrt{(d^2+x^2+y^2)}\right)}{\sqrt{(d^2+x^2+y^2)}} \\ &\approx \frac{1}{d}\exp\left(-i\frac{2\pi}{\lambda}d\right)\exp\left(-i\frac{\pi}{\lambda d}\,(x^2+y^2)\right) \end{aligned} \tag{2.37}$$

$\sqrt{(d^2+x^2+y^2)}$ is the distance between the source point and the point with coordinates (x,y) in the CCD plane. Inserting this expression into reconstruction expression for virtual image, we get,

$$\Gamma(\zeta,\eta) = C\exp\left[+i\frac{\pi}{\lambda d}\,(\xi^2+\eta^2)\right]\Im^{-1}\{h(x,y)\}$$

Where C is a complex constant. Thus lensless Fourier hologram is reconstructed using Fourier transform.

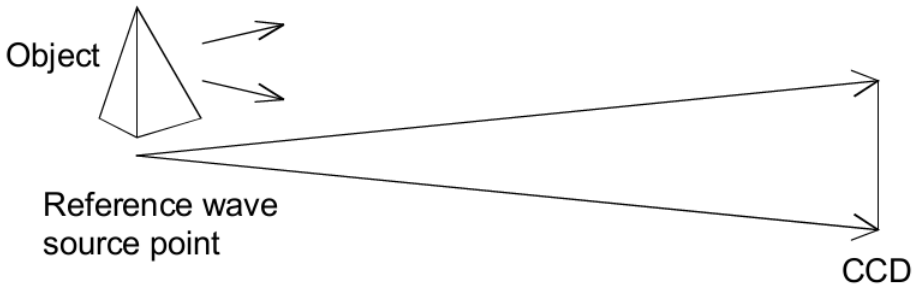

2.38 : Digital lensless Fourier holography[13]

2.7 Separation of DC-term

The bright spot at the center in Figure 2-14 can be seen which the undiffracted reconstruction wave is. All object parts are located behind the zero order or DC term. In order to suppress DC terms, methods are developed[25].

The equation for DC formation can be given by,

$$I(x,y) = |E_0(x,y) + R_R(x,y)|^2$$

$$= a_R^2 + a_0^2 + 2a_R a_0 \cos(\varphi_0 - \varphi_R) \qquad (2.39)$$

First two terms lead to DC terms in the reconstruction process. The average intensity of all pixel of the hologram matrix is,

$$I_m = \frac{1}{N^2} \sum_{k=0}^{N-1} \sum_{l=0}^{N-1} I(k\Delta x, l\Delta y) \qquad (2.40)$$

The terms $a_R^2 + a_0^2$ can be suppressed by subtracting average intensity I_m from the hologram,

$$I'(k\Delta x, l\Delta y) = I(k\Delta x, l\Delta y) - I_m(k\Delta x, l\Delta y) \qquad (2.41)$$

The reconstruction creates an image free of zero order

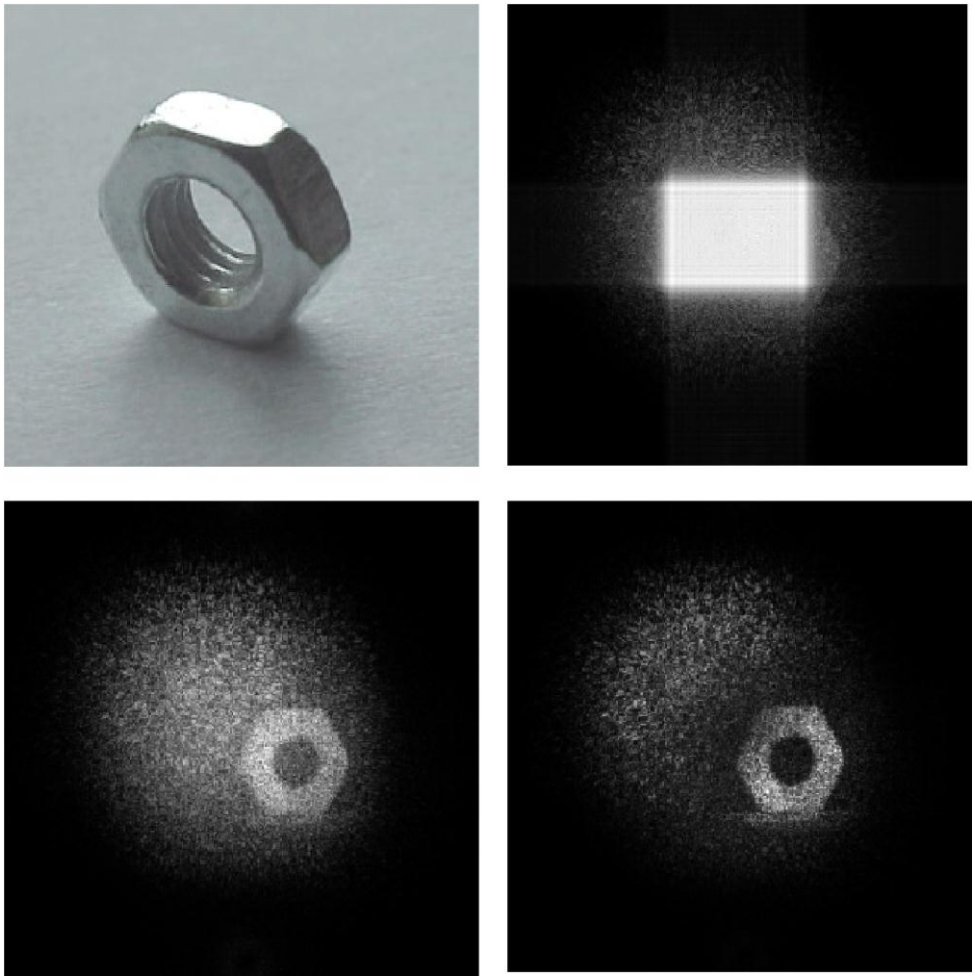

Figure 2-17 : Suppression of the DC term (courtesy of S. Seebacher) [13]

Chapter 3

Lensless Holography

3.1 Introduction

Tools accessible to life scientists, physicians and clinicians to perform light microscopy have continuously improved toward achieving enhanced resolution (both temporally and spatially), better sensitivity and deeper penetration into optically dense media [9], [26]–[34]. With these developments, however, the overall cost and complexity of microscopy modalities have also increased, partially restricting their use in low-resource settings and at the point-of-care. In the meantime, the rapid advancements in digital technologies and consumer electronics have transformed enormously. Today, using broadly available wireless networks and digital processors, we can economically and quickly acquire, transmit and process information, almost anywhere in the World. Undoubtedly, these technological developments are expected to have a strong impact on the design of next generation medical technologies. Building on this foundation, there has been a growing interest in developing new microscopy modalities, which are compact, cost-effective yet sensitive enough for various biomedical imaging applications[32], [35]–[43]. Same way, lensfree computational microscopy takes an alternative approach to image micro-objects on a chip[38]–[43]. In this approach, the basic idea is to replace bulky and costly optical gears, such as microscope objectives and lenses, with digital algorithms to perform high-throughput imaging using significantly miniaturized and cost-effective structures. These techniques can perform complex tasks such as whole blood analysis and imaging of histopathology samples and lot more.

3.2 Optical setup

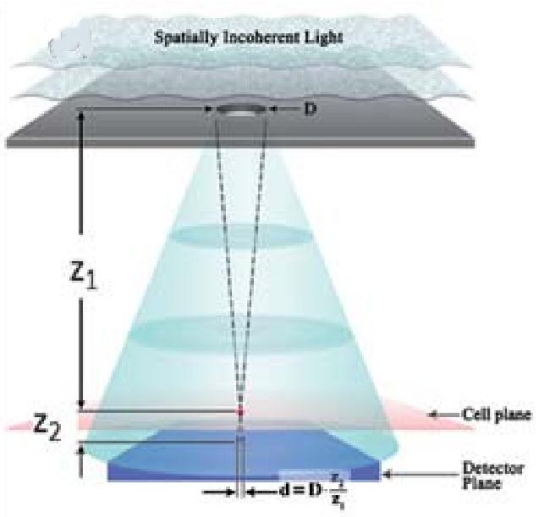

Figure 3-1 : Schematics of the incoherent[36]

Conventional coherent lensfree in-line holography approaches require near-perfect spatial coherence for illumination. It require focusing of a laser light on a small aperture that is on the order of a wavelength for spatial filtering[5], [44].The use of a small aperture size (e.g., 1–2mm) requires a mechanically stable and a carefully aligned system together with a focusing lens to competently couple the laser radiation to the aperture for enhanced light throughput. Keeping such a small aperture clean and operational over an extended period of time can be another challenge especially for field use. The cells of interest are typically positioned far away (e.g., >1 cm) from the sensor surface so that the holographic signature of each cell is spread almost over the entire sensor area, where all the cells' signatures significantly overlap. Unfortunately this approach limits the imaging field-of-view (FOV) at the cell plane. All these requirements not only relatively increase the cost and the size of the optical instrument, but also make lensfree coherent in-line holography somewhat inconvenient for use in resource limited settings[45]

3.3 In-line hologram formation

A finite-spatial-extent wave $A\exp\left(\frac{j2\pi z}{\lambda}\right)$ with amplitude A and wavelength λ propagates from object plane $z = 0$ towards the recording plane $z = d$ where the illuminating intensity is $\left|A\exp\left(\frac{j2\pi d}{\lambda}\right)\right|^2 = |A|^2 = B$ thus provides a coherent background B. if object is placed into the beam at $z = 0$[46]. The wavefront at the object plane can be represented as $U_r(\xi,\eta)$. The

Huygens-Fresnel principle is applied to determine the scalar field distribution $U_h(x,y)$ at the recording plane the field is given by Fresnel diffraction formula[47]

$$U_h(x,y) = \frac{A}{j\lambda d}\exp(jkd)\int_{-\infty}^{\infty}\int_{-\infty}^{\infty} U_r(\xi,\eta) \times \exp\left\{\frac{jk[(x-\xi)^2+(y-\eta)^2]}{2d}\right\} d\xi d\eta. \quad (3.1)$$

Where $k = 2\pi/\lambda$, (ξ,η) and (x,y) are the coordinates at the object plane and recording plane

The hologram can be represented as,

$$H(x,y) = U_h(x,y)U_h^*(x,y) = |A|^2\,|U_r(x,y) \times h_d(x,y)|^2 \quad (3.2)$$

By dividing the hologram image over the background image $H(x,y)/B(x,y)$ the normalized hologram is free of $|A|^2$ thus the influence of light intensity, camera sensitivity, image intensity scale is minimized[48].

3.4 Reconstruction techniques

3.4.1 Image recovery by optimization

3.4.1.1. Image recovery by simulating the physical hologram replay process

The recorded hologram pattern $H(x,y)$(Figure 3-2) is multiplied by conjugate reference beam

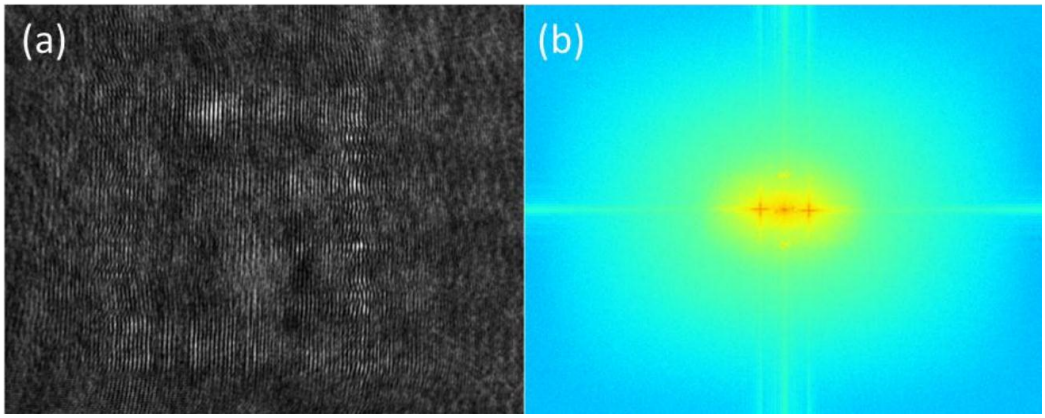

Figure 3-2 : (a) Fresnel hologram of USAF resolution chart; (b) Amplitude of the Fourier transform[49]

and Fresnel back propagate the resultant function to image plane as shown in Figure 3-3 but DC and two cross terms produce overlapping pattern which result in poor image quality

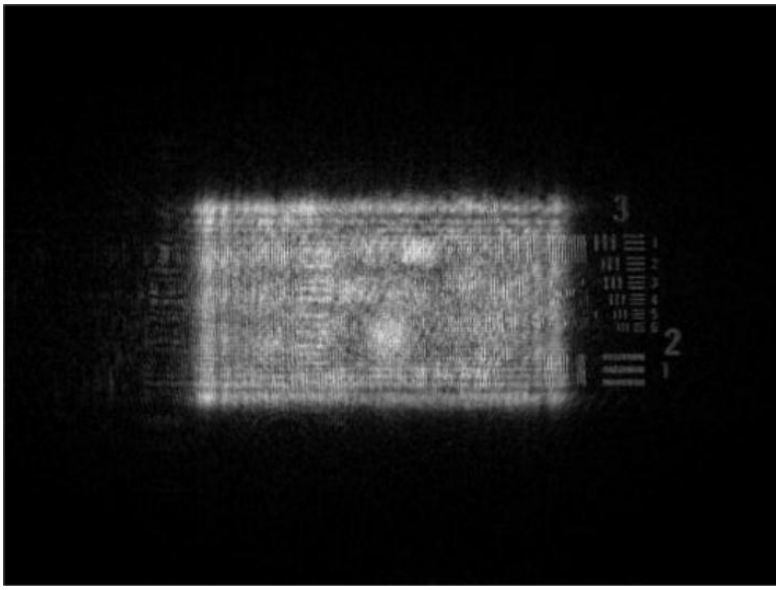

Figure 3-3 : Image recovery by simulating the physical hologram replay process[49]

3.4.1.2. Image recovery by spatial filtering approach

This is another standard method for digital hologram processing. Selecting spatial filter is difficult due to overlapping of the terms. A larger sized spatial filter can improve the image resolution as shown in Figure 3-4 (b) but the recovery has interference from the dc term causing introduction of speckle noise which obscures the high resolution features. For an even larger filter pixels as in Figure 3-4 (e), the corresponding reconstruction in Figure 3-4 (f) is completely obscured by contribution from the dc term. The useful resolution has thus not improved due to the speckle artifacts and/or obscuration due to the dc term when the filter window size is increased. Square shaped filters are used here, any windowing on the filters is not expected to solve the dc term interference problem in this type of approach[49].

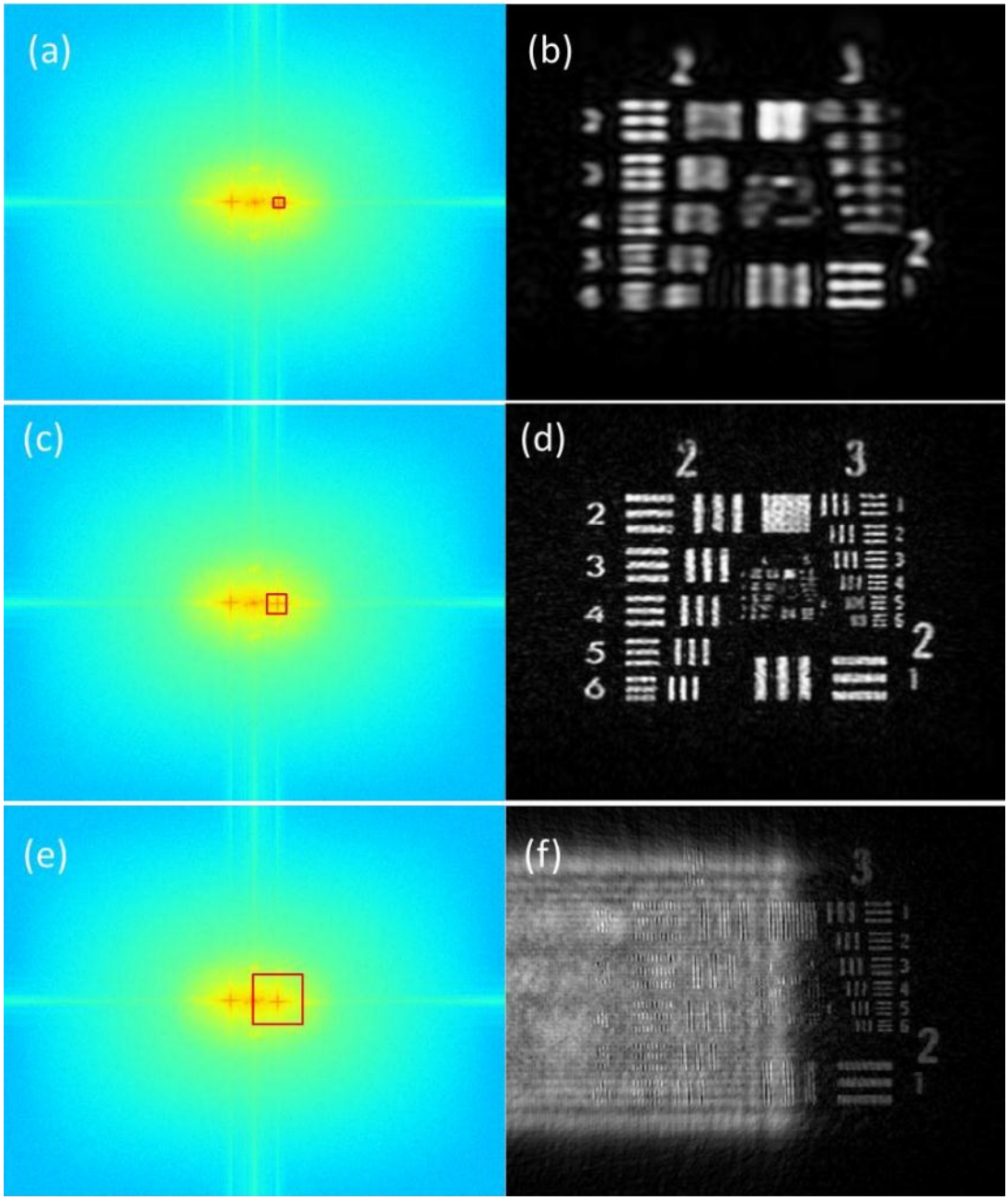

Figure 3-4 :Image recovery using Fourier filtering of hologram[49]

3.4.1.3. Image recovery by solving minimum L2-norm problem

Without smoothing operation, the iteration may be described by

$$O^{(n+1)} = O^{(n)} + t[H - (|O|^2 + |R|^2 + OR^* + O^*R)].(O + R) \qquad (3.3)$$

This iterative procedure provides a complex valued solution $O(x, y)$, starting with the initial guess zero image for the function $O(x, y)$, the solution after 20 iterations is shown in Figure 3-5, where we show the amplitude (Figure 3-5 (a)) and phase (Figure 3-5 (b)) of the

recovered field $O(x, y)$ in the hologram plane. The relative L2-norm error is seen to decrease less than 0.1% in successive iterations by the time 20 iterations are reached.

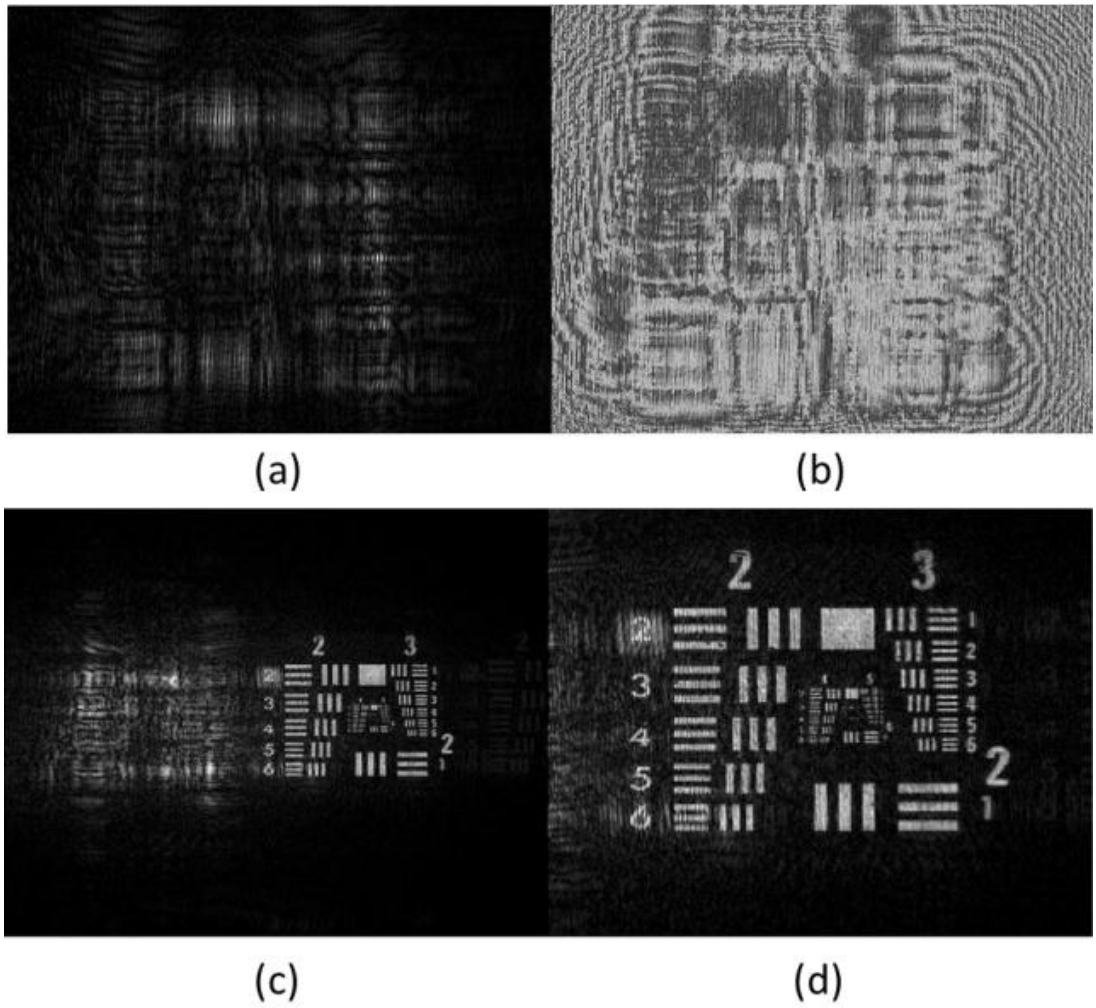

Figure 3-5 : Complex object field and image recovery by solution of minimum L2-norm problem[49]

3.4.1.4. Image recovery by solving minimum L2-norm problem

Although the iterative solution provides a minimum L2-norm solution for the complex field $O(x, y)$ from a single hologram frame, the solution is modulated by the carrier fringes and their harmonics. The modulation on the solution needs to be averaged out in the iterative process to obtain the desired solution which we show next. The iterative procedure is now followed. The carrier fringe period in the recorded hologram (Figure 3-2 (a)) corresponded to 24 pixels on our CMOS array detector. 6(d) show the image recovery after back propagating this field to the object plane. Figure 3-6 (d) is a magnified

version of a part of Figure 3-6 (c). We observe a high quality image recovery without much corruption due to speckle noise. Further, there is no interference from the twin image or the dc terms and as a result the high frequency features in the resolution chart are much more clearly visible

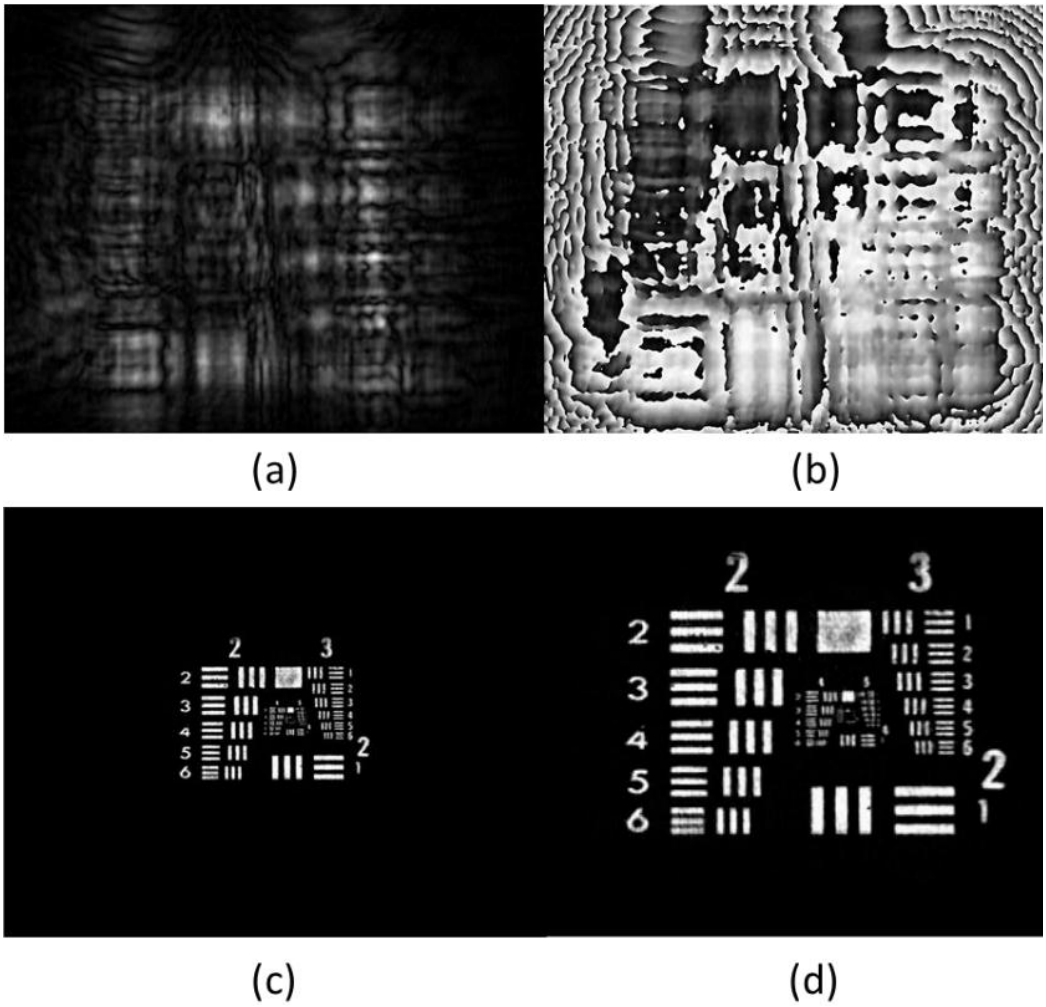

Figure 3-6 : Complex object field and image recovery by solution of constrained optimization[49]

3.4.2 Iterative Method

This algorithm is used to reconstruct $U_r(\xi,\eta)$ in the object plane. The direct reconstruction from the normalized hologram is used as the estimated initial guess to start the iteration. The back and forth propagation between the object and hologram domains is achieved by convolution operation[50]. For object whose phase shift is less than a quarter of the illumination wavelength or illuminated by short wavelength, the constraint on the object domain is non-negative for both real and imaginary part inside the object support, and the

square root of normalized hologram is the magnitude constraint in the recording domain. Reconstruction is shown in following steps:

a) Use the direct reconstruction $U_r^1(\xi,\eta)$ from the normalized hologram as the initial guess.

b) Object edge detection and shape estimations are used to obtain boundary of loose support. In the process, former is obtained by intensity slope's calculation in direct reconstruction using Sobel edge detector[51]

$$\delta S(\xi,\eta) = \alpha, \alpha \in \{|grad|U_r^1(\xi,\eta)|^2|\} \tag{3.4}$$

$S(\xi,\eta)$ denotes loose support and $\delta S(\xi,\eta)$ denotes corresponding boundary.

c) According to the definition of normalized hologram transmission function outside the support is 1.

$$G[U_r^n(\xi,\eta)] = \begin{cases} U_r^n(\xi,\eta) & if\ (\xi,\eta) \in S \\ 1 & otherwise \end{cases} \tag{3.5}$$

d) The real and imaginary parts in the support should be non-negative. Instead of applying a hard projection operation inside the support S, a relaxation β parameter is introduced[52]

$$U_r^n(\xi,\eta) = C[U_r^n(\xi,\eta)](\xi,\eta) \in S \tag{3.6}$$

Where n denotes the number of iteration and C is defined as

$$G[U_r^n(\xi,\eta)] = \begin{cases} U_r^n(\xi,\eta) - \beta \times U_r^n(\xi,\eta) & if\ n = 1 \\ U_r^{-1}(\xi,\eta) - \beta \times U_r^n(\xi,\eta) & if\ n \geq 2 \end{cases} \tag{3.7}$$

Where relaxation parameter β is real and ranges in $0 < \beta < 1$. If $U_r^n(\xi,\eta)$ inside support is negative due to interference between reference wave and twin image the corresponding point of $U_r^n(\xi,\eta)$ grow larger during iterations until all points inside S go non-negative[52]

e) $U_r^n(\xi,\eta)$ propagates to form a new complex field $U_h^n(x,y)$ at the recording plane. The updated complex amplitude at the recording plane is

$$U_h^{n+1}(x,y) = T[U_h^n(x,y)] \tag{3.8}$$

$$T[U_h^n(x,y)] = \sqrt{\frac{H(x,y)}{B(x,y)}} \frac{U_h^n(x,y)}{|U_h^n(x,y)|} \tag{3.9}$$

The transmission function $U_r^{n+1}(\xi,\eta)$ is updated at the object plane. The procedure is repeated from (c) to (e) to form a loop of a concatenation of operators.

$$U_r^{n+1}(\xi,\eta) = CGF_d^- TF_d^+ [U_r^n(\xi,\eta)]$$

$$U_h^{n+1}(x,y) = TF_d^+ CGF_d^- [U_h^n(x,y)] \tag{3.10}$$

Chapter 4

Experiments and Results

In in-line holography, the angle between object wave and reference wave is zero which distinguishes it from the conventional off-axis holography. Large is the angle, better will be the separation between DC term, real image and virtual image in the FFT. Thus reconstruction can be achieved easily in off-axis holography and optimization is require in in-line holography. If the off-axis angle in off-axis holography is reduced to zero, it will lead to the in-line holography, therefore we started with the off-axis holography simulation where off-axis angle was 2^0 then we reduced it to 0.2^0

4.1 Simulations

Hologram (Figure 4-3) of object "H" (Figure 4-1) is created through the simulation with the reference beam at an angle of 2^0 with respect to object beam as shown in Figure 4-2 and reconstructed using optimization technique. The FFT of the hologram before optimization is shown in Figure 4-4, It contains all terms i.e. DC, virtual, and real term, but extent of overlap seen is less, therefore reconstruction can be obtain easily and the amplitude and phase reconstruction before and after optimization are almost same which can be seen in Figure 4-6, Figure 4-7, Figure 4-9 and Figure 4-10.

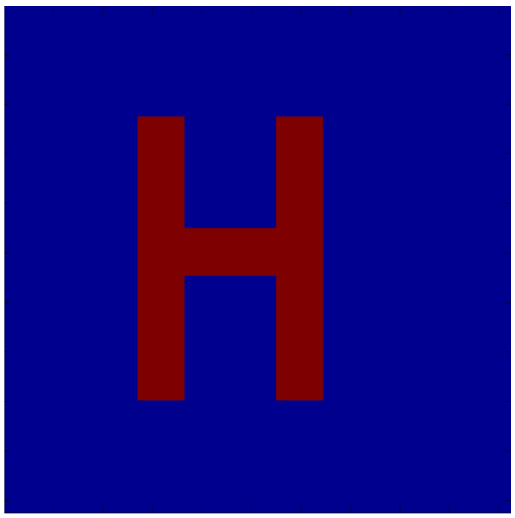

Figure 4-1 : "H" Object

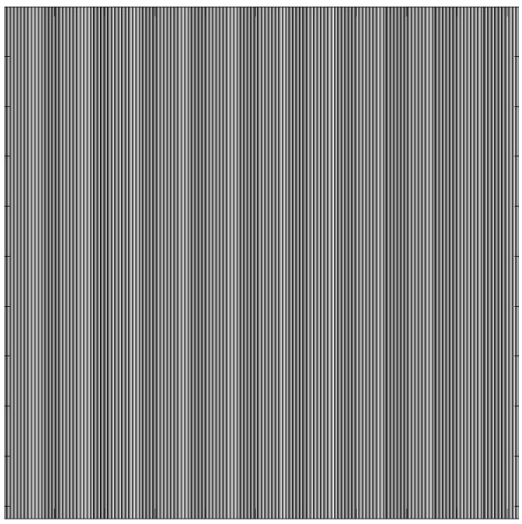

Figure 4-2 : Reference wave illuminated at 2^0

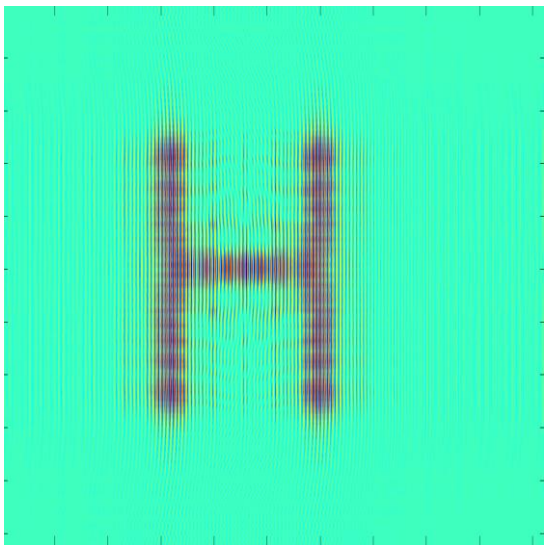

Figure 4-3 : Simulated hologram

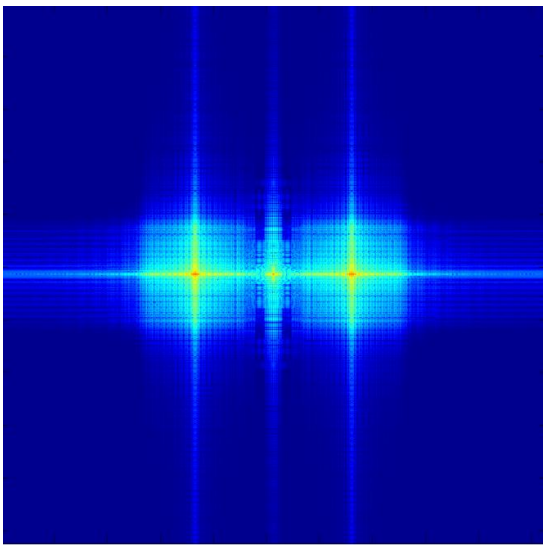

Figure 4-4 : FFT of the hologram

Simulated hologram with "H" object and reference wave at an angle of 2^0 and the its FFT

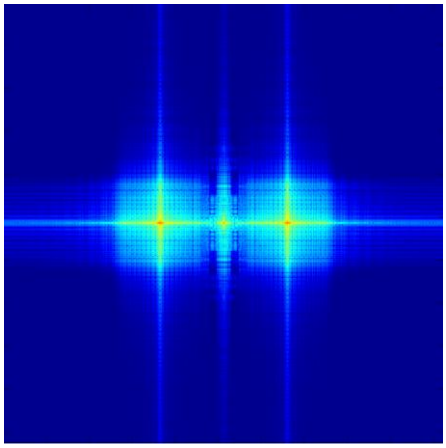

Figure 4-5 : FFT of the hologram

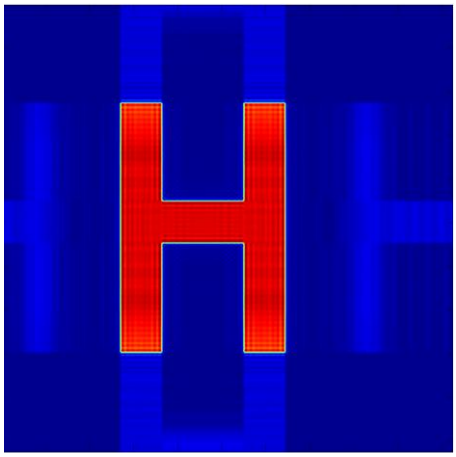

Figure 4-6 : Amplitude Reconstruction

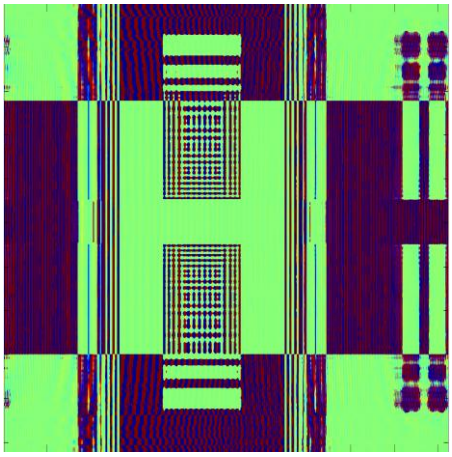

Figure 4-7 : Phase Reconstruction

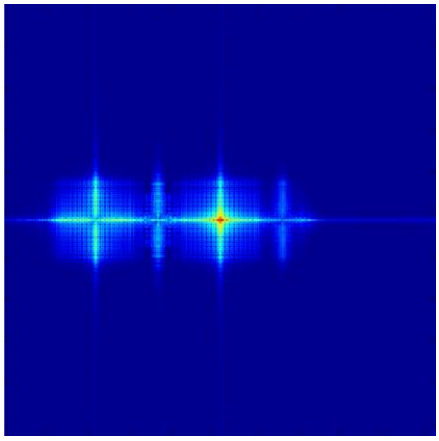

Figure 4-8 : FFT of the recovered object at hologram plane

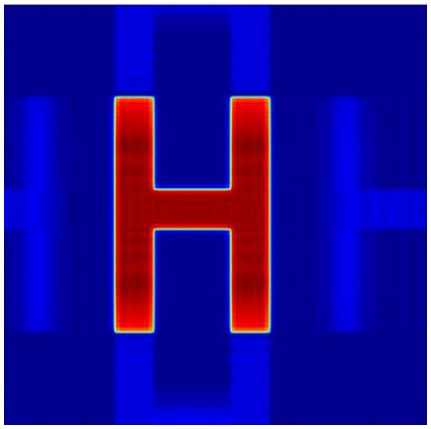

Figure 4-9 Amplitude Reconstruction with recovered object

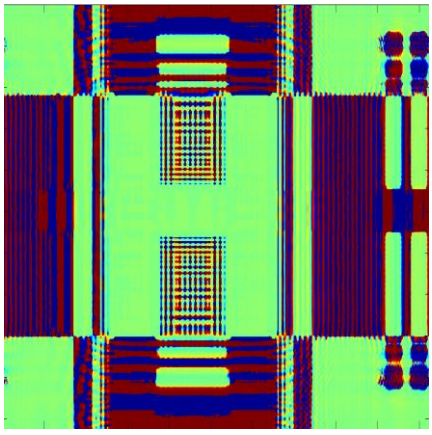

Figure 4-10 : phase reconstruction with recovered object

In another simulation, hologram (Figure 4-14) of object "H" (Figure 4-11) is created through the simulation with the reference beam at an angle of 0.2^0 with respect to object beam as shown in Figure 4-12 and reconstructed using optimization technique. The FFT of the hologram before optimization is shown in Figure 4-14, It contains all terms i.e. DC, virtual, and real term, and the extent of overlap seen is more compared to above case, the image is recovered by optimization, the FFT shows only virtual term Figure 4-18, therefore optimization has great impact when the off-axis angle is less. The difference between amplitude and phase reconstruction before and after optimization can easily be seen in Figure 4-16, Figure 4-17, Figure 4-19 and Figure 4-20

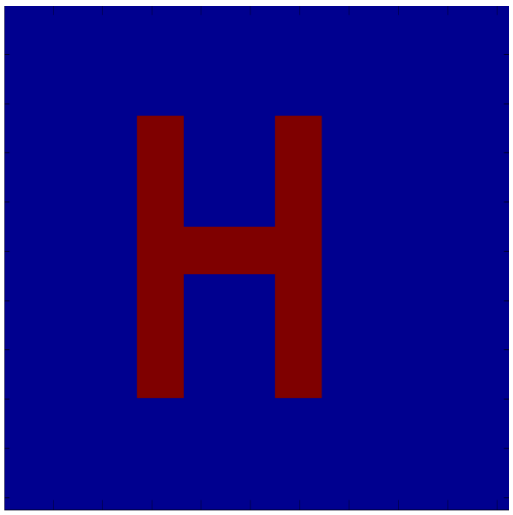

Figure 4-11 : Object

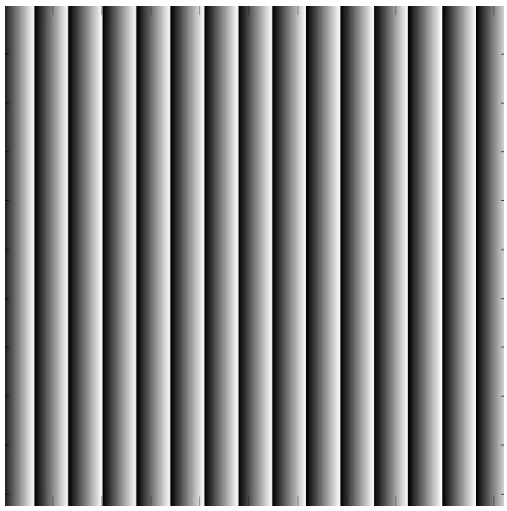

Figure 4-12 : Reference wave at an angle 0.2^0

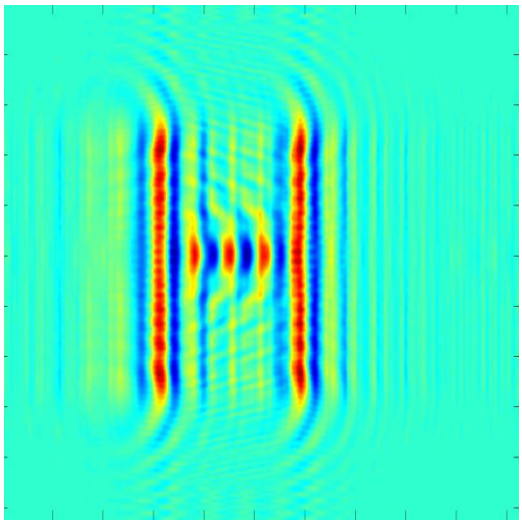

Figure 4-13 : Simulated hologram

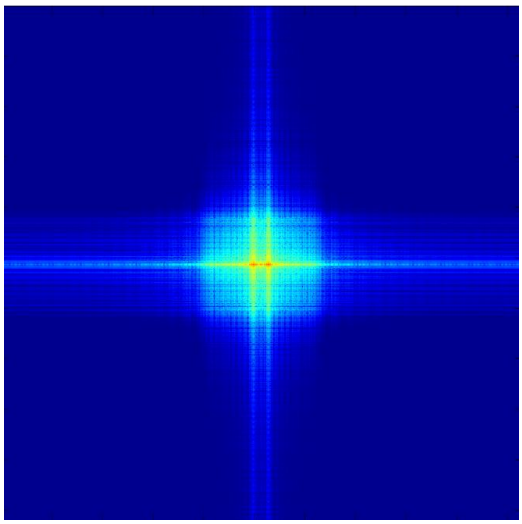

Figure 4-14 : : FFT of the hologram

Simulated Hologram with "H" object and reference wave at an angle of 0.2^0 degrees and its FFT

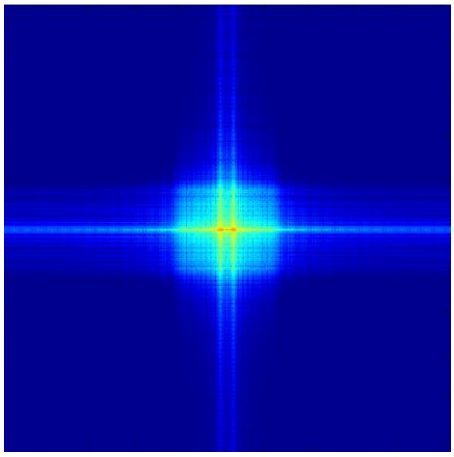

Figure 4-15 : FFT of the hologram

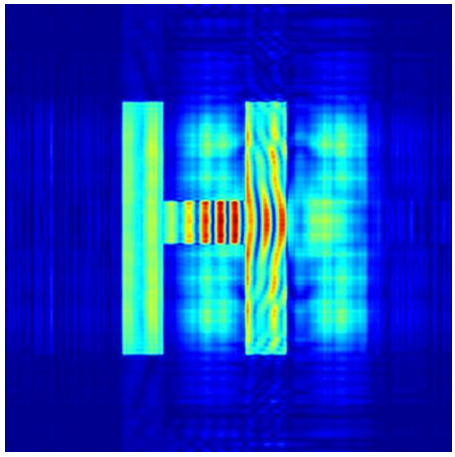

Figure 4-16 : Amplitude Reconstruction

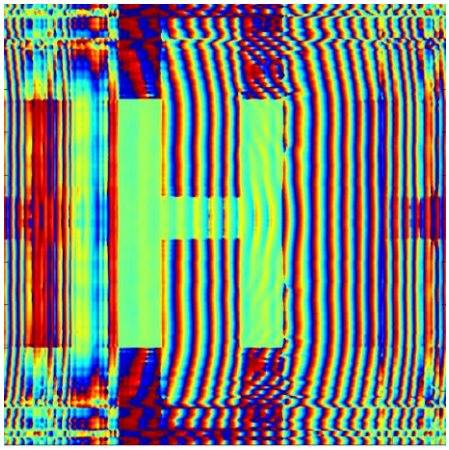

Figure 4-17 : Phase reconstruction

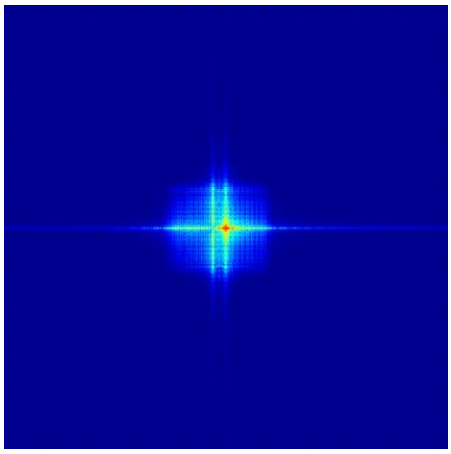

Figure 4-18 : FFT of the recovered object at hologram plane

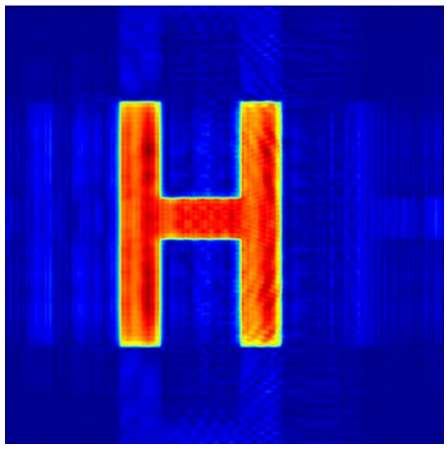

Figure 4-19 : Amplitude reconstruction of the recovered object

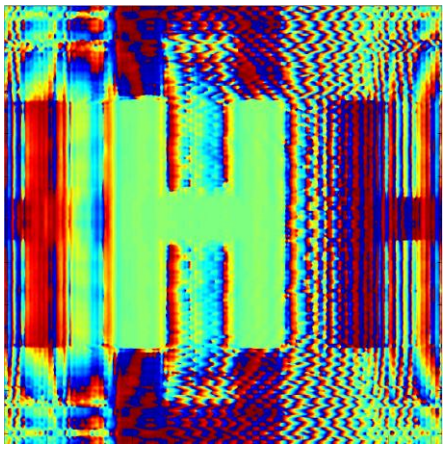

Figure 4-20 : Phase reconstruction of the recovered object

4.2 Off-axis holography

4.2.1 optical Setup

The experimental set-up for DHM is given in the Figure 4-21. 'Nd: YAG' laser with wavelength 532nm is used for illumination. Beam splitter B1 is used to separate the beam into two parts, one is for the object arm and another one is for the reference arm. SP1, SP2 are spatial filters, they are used to remove the random fluctuations in the frequencies. L1 and L2 are lenses used for collimating the beam and micro-object is placed in the object arm, microscopic objective, next to object is used to magnify the micro-size object. Lens L3 is used in the object arm to collimate the beam. Beam splitter B2 is used to make both object beam

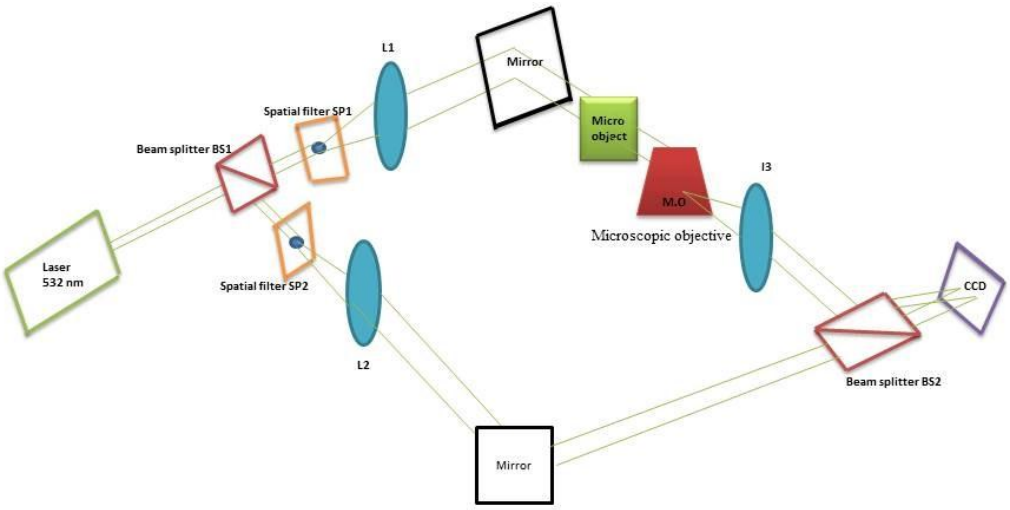

Figure 4-21 : Experimental setup for digital holographic microscopy

and reference beams interfere at the CCD camera at an angle Θ. Thus, interference of two beams create a hologram at CCD. The reconstruction of object is done by multiplying reference wave with the hologram and propagate wave field to the image plane using Fresnel propagation. The Microscopic Objective (MO) magnifies object therefore presence of MO will make digital holography to 'Digital Holographic Microscopy (DHM)

4.2.2 Results

A hologram of object of a letter 'H'is cut at the center of an OHP sheet to act as phase object. It is approximately of the order of 1cm*1cm. In our experiment we illuminated the hologram with laser of wavelength 532 nm. The off-axis angle of reference wave is 2^0, the recorded hologram is shown in the Figure 4-22 along with the reference wave Figure 4-24.

The amplitude and phase reconstruction is given in Figure 4-25and Figure 4-26 respectively. Clearly, the extent of overlap is not significant thus direct reconstruction gives good results. The hologram is further optimized to get the amplitude and phase reconstruction as shown in Figure 4-32and Figure 4-33.

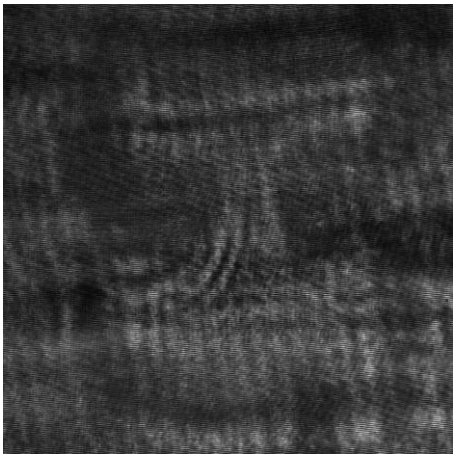

Figure 4-22 : Recorded hologram

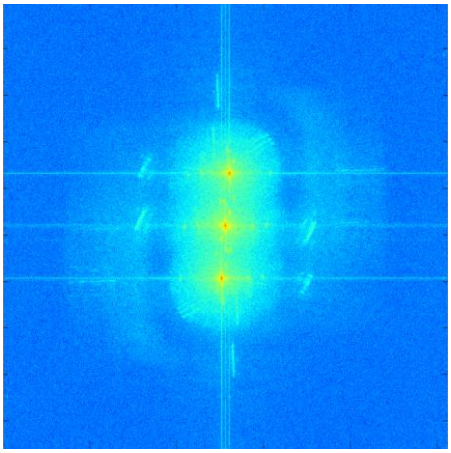

Figure 4-23 : FFT of hologram

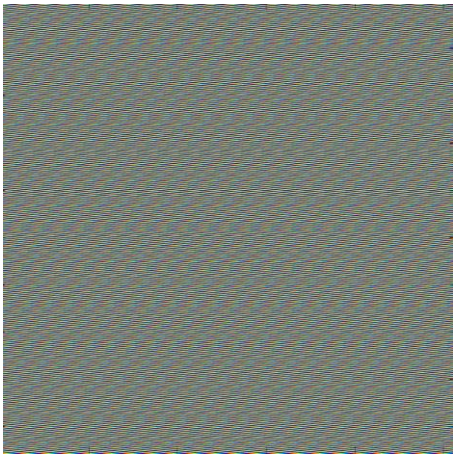

Figure 4-24 : Reference wave at ^{20}

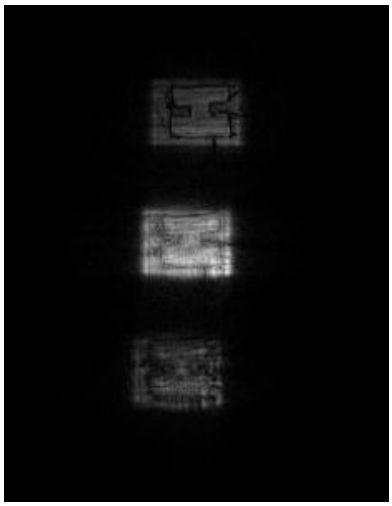

Figure 4-25 : Amplitude reconstruction

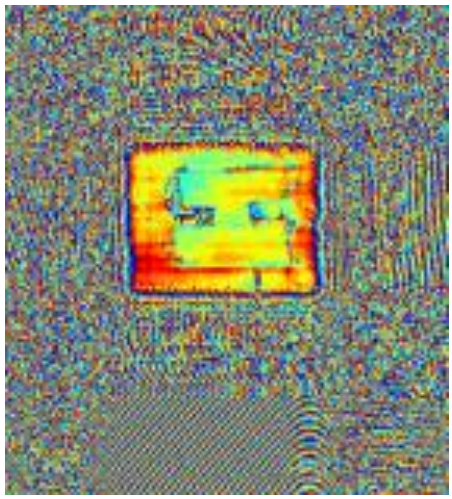

Figure 4-26 : Phase reconstruction

Practical Hologram with "H object" and reference wave at an angle of 2^0 degree and its amplitude and phase reconstruction.

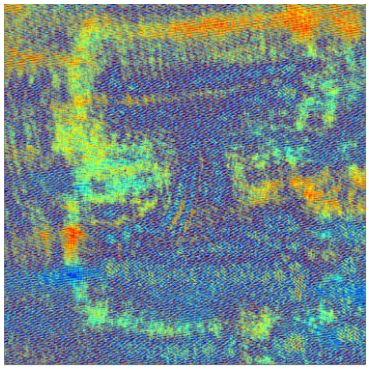

Figure 4-27 : recovered hologram with optimization

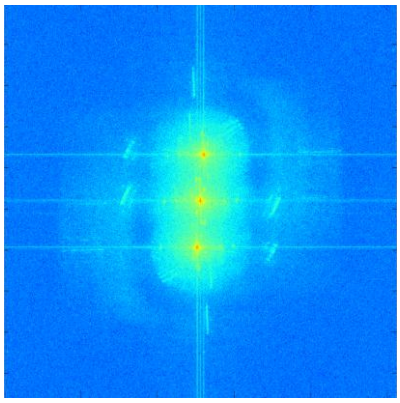

Figure 4-28 : FFT of hologram

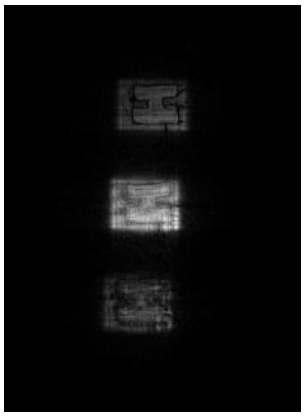

Figure 4-29 : Amplitude reconstruction

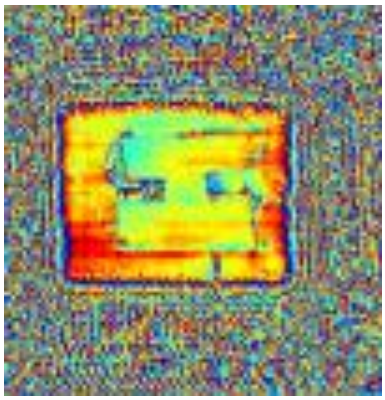

Figure 4-30 : Phase reconstruction

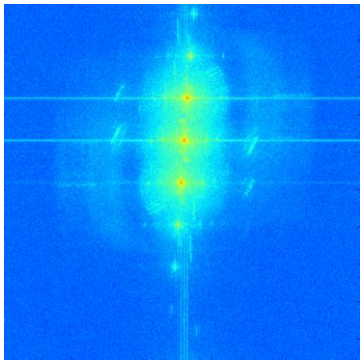

Figure 4-31 : FFT of recovered object at hologram plane

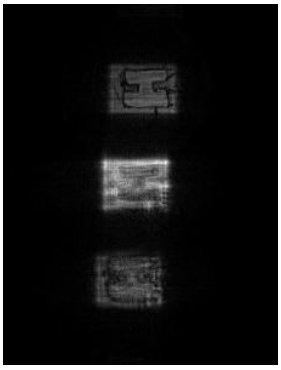

Figure 4-32 : Amplitude reconstruction with recovered object

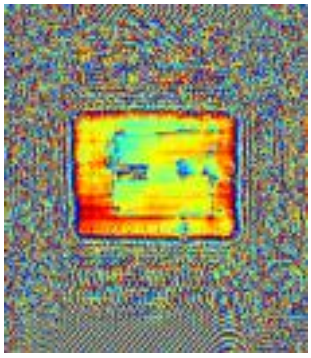

Figure 4-33 : Phase reconstruction with recovered object

4.3 In-line Holography

4.3.1 Optical setup

The object is placed closed to the CCD camera, with typical distance of z2 <5 mm A partially coherent light source, such as an LED (violet), is placed z1 ~4–10 cm away from the objects. Light is filtered by a pinhole of diameter d~25–50 µm to record the digital inline holograms of objects with unit fringe magnification over a large FOV.

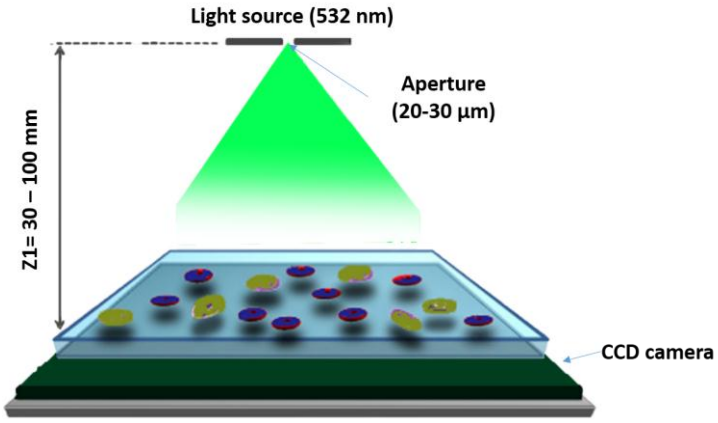

Figure 4-34: Experimental setup for lensless holography

4.3.2 Practical In-line hologram Reconstruction

The sample of agarose beads is used for imaging, which is used for protein purification. The distance between sample and the CCD camera is 3mm. the hologram is illuminated by LED of wavelength 380-450nm.

Figure 4-35 shows the hologram of the object. If we look at the FFT of it, the all components are overlapped as shown in Figure 4 39. The hologram then reconstructed using optimization technique and object is recovered, FFT of which is shown in Figure 4-37. Amplitude and phase reconstruction is shown in Figure 4-38 and Figure 4-39. The result was compared with the image (Figure 4-40) taken by microscope using 50x lens and dimensions were verified.

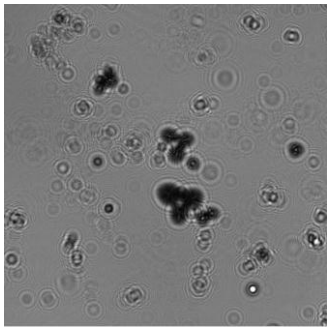

Figure 4-35 : Original hologram

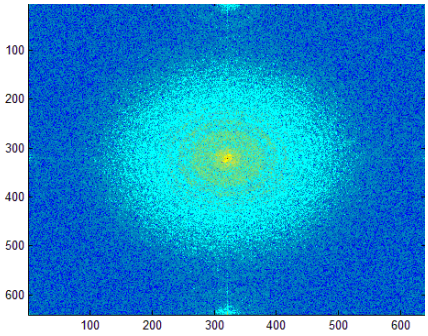

Figure 4-36 : FFT of the hologram

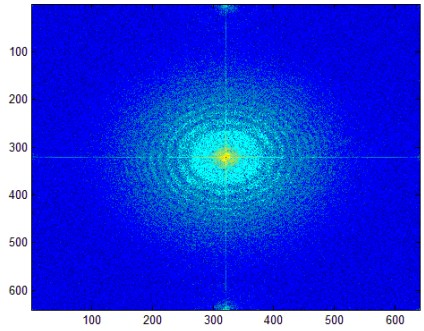

Figure 4-37 : FFT of the recovered hologram

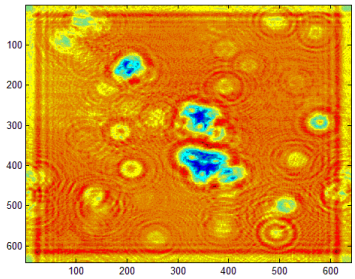

Figure 4-38 : Amplitude reconstruction using optimization

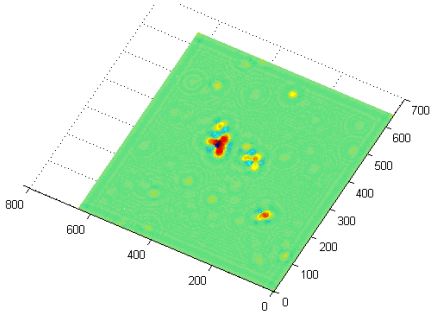

Figure 4-39: Phase Reconstruction using optimization

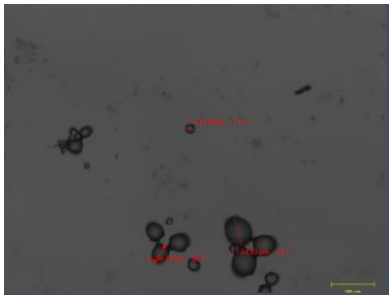

Figure 4-40 : 50x Microscopic view

In another case the same micro beads are used and the impact of optimization is seen. The hologram of the image is shown in Figure 4-41 and is FFT in Figure 4-42 clearly it contains overlap of all components i.e.DC, virtual image and real image.

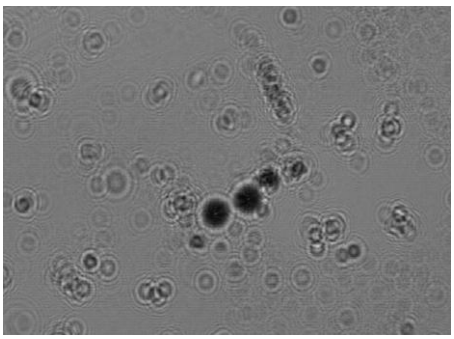

Figure 4-41 : original hologram

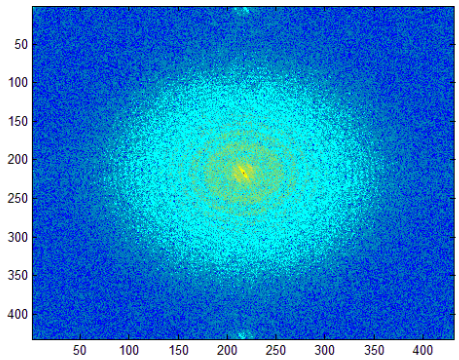

Figure 4-42 : FFT of the hologram

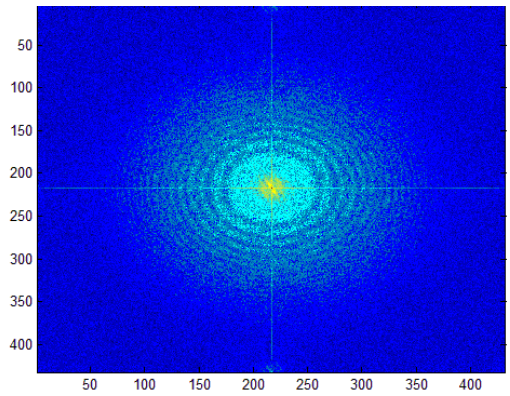

Figure 4-43 : FFT of recovered object

Figure 4-44 and and Figure 4-46 show the amplitude reconstruction before and after optimization respectively. Also Figure 4-45 and Figure 4-47 show the phase reconstruction before and after optimization respectively. Clearly the results after optimization are much better and carry large information.

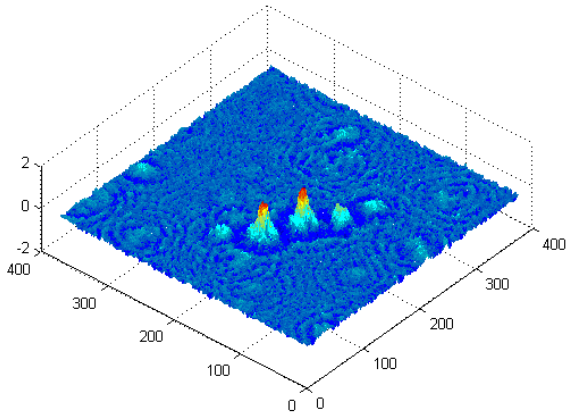

Figure 4-44 : Phase reconstruction without optimization

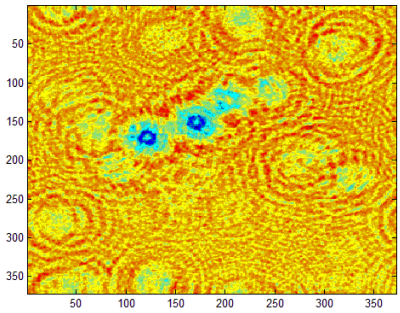

Figure 4-45 : Amplitude reconstruction without optimization

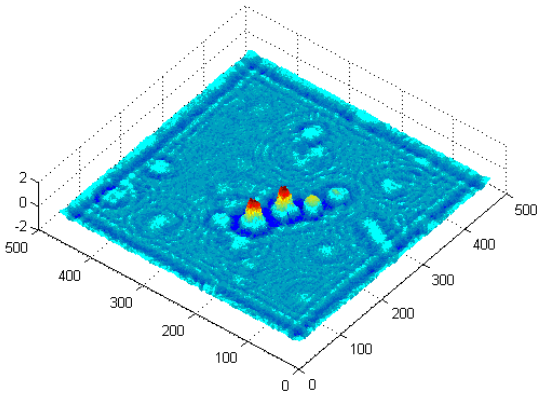

Figure 4-46 : Phase reconstruction with optimization

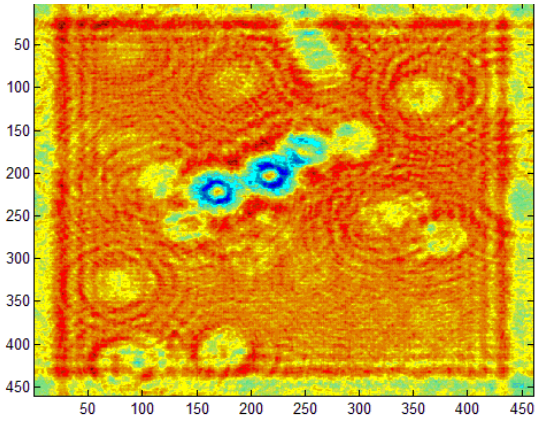

Figure 4-47 : Amplitude reconstruction with optimization

Chapter 5

Summary and Future scope

The “Digital holography microscopy (DHM) is an optical microscopic principle that allows to record the hologram optically and reconstruct the object digitally. Therefore, the speed of reconstruction increases. As explained above there is no need to have additional setup for reconstruction as compared to traditional optical holography. DHM is a growing research field with a strong potential for detection of diseases. Various factors like cost, accuracy and speed of reconstruction are actively under development.

In lensfree in-line holography laser source is replaced by partially coherent LED to obtained same results with reasonable accuracy. Therefore handheld/portable device can be prototyped on the same grounds. The setup can be extended to interface it with cell phone camera to achieve portability and can also be used to monitor microfluidic channels.

References

[1] R. Barretto, B. Messerschmidt, and M. Schnitzer, “In vivo fluorescence imaging with high-resolution microlenses,” *Nat. Methods*, 2009.

[2] W. Choi, C. Fang-Yen, and K. Badizadegan, “Tomographic phase microscopy,” *Nat. …*, 2007.

[3] C. Evans and E. Potma, “Chemical imaging of tissue in vivo with video-rate coherent anti-Stokes Raman scattering microscopy,” *Proc. …*, 2005.

[4] J. Rosen and G. Brooker, “Non-scanning motionless fluorescence three-dimensional holographic microscopy,” *Nat. Photonics*, 2008.

[5] W. Xu and M. Jericho, “Digital in-line holography for biological applications,” *Proc. …*, 2001.

[6] D. Psaltis, S. Quake, and C. Yang, “Developing optofluidic technology through the fusion of microfluidics and optics,” *Nature*, 2006.

[7] G. Pedrini and H. Tiziani, “Short-coherence digital microscopy by use of a lensless holographic imaging system,” *Appl. Opt.*, 2002.

[8] W. Haddad, D. Cullen, and J. Solem, “Fourier-transform holographic microscope,” *Appl. …*, 1992.

[9] K. Goda, K. Tsia, and B. Jalali, “Serial time-encoded amplified imaging for real-time observation of fast dynamic phenomena,” *Nature*, 2009.

[10] D. GABOR, “A New Microscopic Principle,” *Nature*, vol. 161, no. 4098, pp. 777–778, May 1948.

[11] D. Gabor, “Microscopy by Reconstructed Wave-Fronts,” *Proc. R. Soc. A Math. Phys. Eng. Sci.*, vol. 197, no. 1051, pp. 454–487, Jul. 1949.

[12] D. Gabor, “Microscopy by Reconstructed Wave Fronts: II,” *Proc. Phys. Soc. Sect. B*, vol. 64, no. 6, pp. 449–469, Jun. 1951.

[13] U. Schnars and W. Jueptner, *Digital holography*. 2005.

[14] E. N. LEITH and J. UPATNIEKS, “Wavefront Reconstruction with Diffused Illumination and Three-Dimensional Objects,” *J. Opt. Soc. Am.*, vol. 54, no. 11, p. 1295, Nov. 1964.

[15] E. N. LEITH and J. UPATNIEKS, “Reconstructed Wavefronts and Communication Theory,” *J. Opt. Soc. Am.*, vol. 52, no. 10, p. 1123, Oct. 1962.

[16] J. W. Goodman, “DIGITAL IMAGE FORMATION FROM ELECTRONICALLY DETECTED HOLOGRAMS,” *Appl. Phys. Lett.*, vol. 11, no. 3, p. 77, Nov. 1967.

[17] M. A. Kronrod, N. S. Merzlyakov, and L. P. Yaroslavskii, “Reconstruction of a Hologram with a Computer,” *Sov. Phys. Tech. Phys.*, vol. 17, 1972.

[18] U. Schnars and W. Jüptner, “Principles of direct holography for interferometry,” *Proc. 2nd Int. Work. …*, 1993.

[19] U. Schnars and W. Jüptner, “Direct recording of holograms by a CCD target and numerical reconstruction,” *Appl. Opt.*, 1994.

[20] U. Schnars and W. Jüptner, “Digital recording and numerical reconstruction of holograms,” *Meas. Sci. Technol.*, 2002.

[21] Schnars, Ulf, and W. Jueptner, *Digital holography*. Springer Berlin Heidelberg, 2005.

[22] U. Schnars, “Direct phase determination in hologram interferometry with use of digitally recorded holograms,” *J. Opt. Soc. Am. A*, vol. 11, no. 7, p. 2011, Jul. 1994.

[23] U. Schnars, “Digitale Aufzeichnung und mathematische Rekonstruktion von Hologrammen,” 1994.

[24] T. Demetrakopoulos and R. Mittra, “Digital and optical reconstruction of images from suboptical diffraction patterns,” *Appl. Opt.*, 1974.

[25] T. Kreis and W. Ju, “Suppression of the dc term in digital holography,” *Opt. Eng.*, 1997.

[26] E. Cuche, F. Bevilacqua, and C. Depeursinge, “Digital holography for quantitative phase-contrast imaging,” *Opt. Lett.*, 1999.

[27] E. Betzig, G. Patterson, and R. Sougrat, “Imaging intracellular fluorescent proteins at nanometer resolution,” *Science (80-.).*, 2006.

[28] S. Hell, “Toward fluorescence nanoscopy,” *Nat. Biotechnol.*, 2003.

[29] M. Gustafsson, “Nonlinear structured-illumination microscopy: wide-field fluorescence imaging with theoretically unlimited resolution,” *Proc. Natl. Acad. …*, 2005.

[30] S. Hess, T. Girirajan, and M. Mason, “Ultra-high resolution imaging by fluorescence photoactivation localization microscopy,” *Biophys. J.*, 2006.

[31] M. Rust, M. Bates, and X. Zhuang, “Sub-diffraction-limit imaging by stochastic optical reconstruction microscopy (STORM),” *Nat. Methods*, 2006.

[32] W. Zipfel, R. Williams, and W. Webb, “Nonlinear magic: multiphoton microscopy in the biosciences,” *Nat. Biotechnol.*, 2003.

[33] E. Chung, D. Kim, Y. Cui, Y. Kim, and P. So, “Two-dimensional standing wave total internal reflection fluorescence microscopy: superresolution imaging of single molecular and biological specimens,” *Biophys. J.*, 2007.

[34] Y. Sung, W. Choi, and C. Fang-Yen, “Optical diffraction tomography for high resolution live cell imaging,” *Opt. ...*, 2009.

[35] S. Seo, S. Isikman, and I. Sencan, “High-throughput lens-free blood analysis on a chip,” *Anal. ...*, 2010.

[36] D. Tseng, O. Mudanyali, and C. Oztoprak, “Lensfree microscopy on a cellphone,” *Lab Chip*, 2010.

[37] W. Bishara, T. Su, A. Coskun, and A. Ozcan, “Lensfree on-chip microscopy over a wide field-of-view using pixel super-resolution,” *Opt. Express*, 2010.

[38] O. Mudanyali, C. Oztoprak, D. Tseng, A. Erlinger, and A. Ozcan, “Detection of waterborne parasites using field-portable and cost-effective lensfree microscopy,” *Lab Chip*, 2010.

[39] H. Zhu, O. Yaglidere, T. Su, D. Tseng, and A. Ozcan, “Cost-effective and compact wide-field fluorescent imaging on a cell-phone,” *Lab Chip*, 2011.

[40] T. Su, A. Erlinger, D. Tseng, and A. Ozcan, “Compact and light-weight automated semen analysis platform using lensfree on-chip microscopy,” *Anal. Chem.*, 2010.

[41] “Holographic pixel super-resolution in portable lensless on-chip microscopy using a fiber-optic array,” *Lab Chip*, 2011.

[42] S. Isikman, W. Bishara, U. Sikora, and O. Yaglidere, “Field-portable lensfree tomographic microscope,” *Lab Chip*, 2011.

[43] S. Isikman, W. Bishara, H. Zhu, and A. Ozcan, “Optofluidic tomography on a chip,” *Appl. Phys. Lett.*, 2011.

[44] J. Garcia-Sucerquia, W. Xu, and S. Jericho, “Digital in-line holographic microscopy,” *Appl. ...*, 2006.

[45] “Compact, light-weight and cost-effective microscope based on lensless incoherent holography for telemedicine applications,” *Lab Chip*, 2010.

[46] L. Rong, Y. Li, S. Liu, W. Xiao, F. Pan, and D. Wang, “Iterative solution to twin image problem in in-line digital holography,” *Opt. Lasers Eng.*, vol. 51, no. 5, pp. 553–559, 2013.

[47] J. W. Goodman, “<italic>Introduction to Fourier Optics, Second Edition</italic>,” *Opt. Eng.*, vol. 35, no. 5, p. 1513, May 1996.

[48] M. Maleki and A. Devaney, “Noniterative reconstruction of complex-valued objects from two intensity measurements,” *Opt. Eng.*, 1994.

[49] K. Khare, P. T. S. Ali, and J. Joseph, “Single shot high resolution digital holography.,” *Opt. Express*, vol. 21, no. 3, pp. 2581–91, 2013.

[50] J. Goodman, *Introduction to Fourier optics*. 2005.

[51] R. C. Gonzalez, R. E. Woods, and S. L. Eddins, *Digital Image Processing Using MATLAB*. Pearson Education, 2004.

[52] J. Fienup, “Phase retrieval algorithms: a comparison,” *Appl. Opt.*, 1982.